

Ternary Metal Oxides based Electron Transport Layers for Perovskite Solar Cells



By

Saad Nadeem

Reg No. 00000330175

Session 2020-2022

Supervised by

Dr. Nadia Shahzad

US-Pakistan Center for Advanced Studies in Energy (USPCAS-E)

National University of Sciences and Technology (NUST)

H-12, Islamabad 44000, Pakistan

July 2023

Ternary Metal Oxides based Electron Transport Layers for Perovskite Solar Cells



By

Saad Nadeem

Reg No. 0000330175

Session 2020-2022

Supervised by

Dr. Nadia Shahzad

**A Thesis Submitted to the US-Pakistan Center for Advanced Studies in
Energy in partial fulfillment of the requirements for the degree of
MASTER of SCIENCE in
ENERGY SYSTEMS ENGINEERING**

US-Pakistan Center for Advanced Studies in Energy (USPCAS-E)

National University of Sciences and Technology (NUST)

H-12, Islamabad 44000, Pakistan

July 2023


THESIS ACCEPTANCE CERTIFICATE

Certified that final copy of MS thesis written by **Mr. Saad Nadeem** (Registration No. 00000330175), of U.S.-Pakistan Center for Advanced Studies in Energy has been vetted by undersigned, found complete in all respects as per NUST Statues/Regulations, is within the similarity indices limit and is accepted as partial fulfillment for the award of MS degree. It is further certified that necessary amendments as pointed out by GEC members of the scholar have also been incorporated in the said thesis.


Signature:  _____

Name of Supervisor: Dr. Nadia Shahzad

Date: 27/07/23

Signature (HoD):  _____

Date: 27/7/2023

Signature (Dean/Principal):  _____

Date: 27/7/2023

CERTIFICATE

This is to certify that work in this thesis has been carried out by **Mr. Saad Nadeem** and completed under my supervision in Solar Energy Research laboratory, US-Pakistan Center for Advanced Studies in Energy (USPCAS-E), National University of Sciences and Technology, H-12, Islamabad, Pakistan.

Supervisor:




Dr. Nadia Shahzad
USPCAS-E
NUST, Islamabad

GEC member 1:



Dr. Rabia Liaquat
USPCAS-E
NUST, Islamabad

GEC member 2:



Dr. Sehar Shakir
USPCAS-E
NUST, Islamabad

GEC member 3:



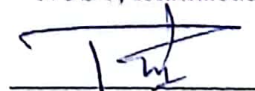
Dr. M. Imran Shahzad
NS & TD (NCP, ISB)

HOD-ESE/TEE/EPE:



Dr. Rabia Liaquat
USPCAS-E
NUST, Islamabad

Dean/Principal:



Dr. Adeel Waqas
USPCAS-E
NUST, Islamabad

Dedication

*With Allah's light, my path defined,
Mercy and wisdom intertwined,
His endless grace, forever enshrined,
A beacon in darkness, ever kind.*

*To parents, who nurtured, held me high,
Their love and support, my endless supply,
A debt of gratitude, words can't imply,
Their sacrifices, I'll never deny.*

*Friends, steadfast, in laughter and tears,
Their presence, a balm for all my fears,
Through struggles, they've been my peers,
Cherished companions, throughout the years.*

*In gratitude, this thesis I pen,
To all who've inspired, now and then,
A humble tribute, to hearts I've touched,
A verse of thanks, in knowledge thrust.*

Acknowledgement

First and foremost, I express my deepest gratitude to **Almighty Allah**, the Creator of everything. And all respects for His **Prophet Muhammad** (PBUH, On Whom Be Allah's Blessings and Salutations). Without His divine blessings, this diligent and challenging task would have been impossible.

I wholeheartedly thank my supervisor, **Dr. Nadia Shahzad**, for her unwavering support, guidance, and invaluable experience in research. Her generosity in sharing her knowledge, providing freedom to explore research ideas, and fostering my research intuition has been instrumental in the completion of this work. I am eternally grateful for her kindness and patience throughout this journey.

I seize this opportunity to express my appreciation to all the Department faculty members for their assistance and encouragement. My special thanks extend to the lab engineers for their guidance during my work, as well as to my lab fellows for their continuous support during the long hours spent at the Solar Energy Research Lab.

Lastly, I convey my heartfelt regards to my GEC members for their steadfast support and guidance throughout this research project. I am also grateful to USPCAS-E for allowing me to use their state-of-the-art lab facilities. This thesis stands as a testament to the collective wisdom, dedication, and perseverance of all who have contributed to its completion.

Saad Nadeem

Abstract

Perovskite solar cells (PSCs) have acquired popularity owing to their high efficiency, ease of fabrication, and affordability. Within this context, there has been a considerable focus on the development of electron transport layers (ETLs) for highly efficient planar photovoltaic devices. This study investigates the potential of zinc-tin based ternary metal oxide ETLs for their application in planar PSCs. To achieve this, the study employed solution-processed method to fabricate three types of ETL films: crystalline zinc stannate (Zn_2SnO_4), amorphous zinc-tin oxide (ZTO), and a bilayer film composed of Zn_2SnO_4 and ZTO. The structural, morphological, and optoelectronic properties of these films were thoroughly examined. X-ray diffraction (XRD) and scanning electron microscopy (SEM) images showed enhanced crystallite size and better surface morphology of perovskite films deposited on bilayer ETL. These ETLs exhibited uniform coverage and high transmittance of up to 90% in the visible spectrum with a band gap range from 4.14 eV for ZTO ETL to 4.29 eV for bilayer ETL. Whereas Photoluminescence studies and Hall effect measurements revealed superior charge extraction, an improved charge carrier mobility ($21.84 \text{ cm}^2\text{V}^{-1}\text{s}^{-1}$) and enhanced n-type conductivity in the bilayer ETL. Moreover, the contact angle analysis of the perovskite layer deposited on the bilayer ETL demonstrated increased resistance to moisture erosion, as indicated by the contact angle of 52.20° . This finding is particularly significant considering the detrimental effects that moisture can have on the performance of PSCs.

Keywords: ternary metal oxides, electron transport layer, perovskite solar cells, bilayer, ambient fabrication.

Table of Contents

Abstract	vii
List of Figures.....	xi
List of Tables	xiii
Publications	xiv
List of Abbreviations	xv
Chapter 1 Introduction	1
1.1 Fossil Fuels and Climate Change.....	1
1.2 Impacts of Climate Change in Pakistan	1
1.3 Renewable Energy: Potential and Policies in Pakistan	2
1.4 History of Solar PV Cells	3
1.5 Perovskite Solar Cells	4
1.5.1 Working Principle	4
1.5.2 Device Architecture	5
1.6 Electron Transport Layers (ETLs)	6
1.6.1 Role of ETLs in Perovskite Solar Cells	7
1.6.2 Types of Electron Transport Layers	7
1.7 Problem Statement	7
1.8 Research Objectives	8
Summary	9
References	10
Chapter 2 Literature Review	13
2.1 Characteristics of Metal Oxide Electron Transport Layers	13
2.1.1 Electronic Properties	13
2.1.2 Optical Properties	14
2.1.3 Morphology Control	15
2.1.4 Chemical Stability	15
2.2 Binary and Ternary Metal Oxide Electron Transport Layers	16
2.2.1 Binary Metal Oxide ETLs	16
2.2.2 Ternary Metal Oxide ETLs.....	17
2.3 Bi-layer Metal Oxide Electron Transport Layers.....	18

2.3.1 Deposition Methods of Metal Oxide Electron Transport Layers	18
2.3.1.1 Solution Process Method	18
2.3.1.2 Atomic Layer Deposition	21
2.3.1.3 Chemical Bath Deposition	22
2.3.1.4 Other Deposition Methods	22
2.4 Evolution of Bilayer Ternary Metal Oxide ETLs	23
2.4.1 Unexplored Avenues in Research	23
2.4.2 Proposed Action Plan	24
Summary	25
References	26
Chapter 3 Introduction to Deposition and Characterization Techniques	35
3.1 Deposition Methods	35
3.1.1 Spin Coating	35
3.1.2 Glove Box	36
3.1.3 Plasma Cleaning	37
3.2 Characterization Techniques	38
3.2.1 UV-Vis-NIR Spectroscopy	38
3.2.2 Scanning Electron Microscopy (SEM)	39
3.2.3 X-Ray Diffraction (XRD)	40
3.2.4 Hall Effect Measurement System	41
3.2.5 Contact Angle Measurement System	42
3.2.6 Photoluminescence (PL) Spectroscopy	43
Summary	45
References	46
Chapter 4 Experimental Work	49
4.1 Materials	49
4.2 Preparation of ETLs	49
4.3 Preparation and Deposition of Absorber Layer	50
4.4 Film Characterizations	51
4.4.1 X-Ray Diffraction (XRD)	51
4.4.2 Scanning Electron Microscopy (SEM)	51
4.4.3 UV-Vis-NIR Spectroscopy	52

4.4.4 Hall Effect Measurement	52
4.4.5 Contact Angle Measurement	52
4.4.6 Photoluminescence (PL) Analysis	52
Flowchart.....	53
Summary	54
Chapter 5 Results and Discussion	55
5.1 Structural Analysis	55
5.2 Morphological Analysis	58
5.3 Optical and Electrical Properties	59
5.4 Photoluminescence (PL) Analysis	62
5.5 Wettability Study.....	63
Summary	65
References	66
Chapter 6 Conclusions and Recommendations.....	69
6.1 Conclusions.....	69
6.2 Future Recommendations	69
Summary	71
Appendix-A: Journal Article	72
Appendix-B: Journal Article	73

List of Figures

Figure 1.1 Projections for Pakistan (2050): a) Record high temperature, b) Impact on precipitation.....	02
Figure 1.2 Working principle of perovskite solar cell (PSC)	05
Figure 1.3 Different structures of a PSC: (a) Planar (n-i-p), (b) inverted planar (p-i-n) .	06
Figure 2.1 a) Schematic diagram of carrier injection and collection in PSCs. b) Important factors for ideal electron transport layers	14
Figure 2.2 Depiction of common techniques for depositing MO ETLs: a) solution process b) atomic layer deposition c) chemical bath deposition and d) magnetron sputtering	21
Figure 3.1 Different processes taking place in the spin coating of thin films	36
Figure 3.2 Glove Box Setup	37
Figure 3.3 Plasma Cleaner.....	37
Figure 3.4 Working principle of UV-Vis-NIR spectrophotometer: a) Single beam setup, b) double beam setup	39
Figure 3.5 Schematic of basic SEM Components	40
Figure 3.6 Atomic-level illustration of the X-ray interaction with the sample following Bragg's Law	41
Figure 3.7 Hall Effect Measurement System	42
Figure 3.8 Contact angle measurement system working principle schematic	43
Figure 3.9 Working principle of photoluminescence spectroscopy.....	44

Figure 4.1 Methodology for the preparation of ZTO, ZS and Bilayer electron transport layers.	50
Figure 4.2 Schematic illustration of perovskite layer deposition	51
Figure 5.1 XRD Spectra of a) bare FTO, ZTO ETL, ZS ETL and Bilayer ETL. b) Perovskite layer coated on FTO, ZTO ETL, ZS ETL and Bilayer ETL. c) Crystallite Size and d) Dislocation Density of perovskite layer deposited on bare FTO, ZS, ZTO and Bilayer ETLs	55
Figure 5.2 XRD Spectrum of ZTO ETL on Glass Substrate.....	56
Figure 5.3 Top-view SEM images of (a) ZTO ETL (b) ZS ETL (c) Bilayer ETL coated on FTO substrate. Top-view SEM images of $\text{Cs}_{0.1}\text{MA}_{0.9}\text{Pb}(\text{I}_{0.9}\text{Br}_{0.1})_3$ deposited on (d) ZTO ETL (e) ZS ETL and (f) Bilayer ETL	58
Figure 5.4 (a) Transmittance spectra of ternary metal oxides and bilayer ETLs. (b) Tauc plots of ternary metal oxides and bilayer ETLs.....	59
Figure 5.5 Absorbance spectra of perovskite film coated on glass, ZTO, ZS and Bilayer ETLs.....	60
Figure 5.6 Urbach Energies (E_u) of perovskite film coated on glass and different ETLs	61
Figure 5.7 Photoluminescence spectrum (PL) of the perovskite film on Glass, ZTO, ZS and Bilayer ETLs	62
Figure 5.8 Water contact angle of (a) ZS ETL (b) ZTO ETL (c) Bilayer ETL and water contact angle of $\text{Cs}_{0.1}\text{MA}_{0.9}\text{Pb}(\text{I}_{0.9}\text{Br}_{0.1})_3$ perovskite film coated on (d) ZS ETL (e) ZTO ETL and (f) Bilayer ETL.....	63
Figure 5.9 Water contact angle of (a) bare glass substrate and (b) pristine perovskite film deposited on glass substrate	64

List of Tables

Table 1 Photovoltaic performances of PSC devices with multi-layer ETLs	19
Table 2 Crystallographic parameters of perovskite absorber layer deposited on bare FTO, ZS, ZTO and Bilayer ETLs	57
Table 3 Hall Effect parameters of different ternary metal oxide based ETLs	62

Publications

1. **Saad Nadeem**; Nadia Shahzad; Sana Mehmood; Muhammad Salik Qureshi; Abdul Sattar; Rabia Liaquat; Sehar Shakir; Muhammad Imran Shahzad, “**Solution-processed Zn_2SnO_4 / ZTO electron transport layers for planar perovskite solar cells**”, *Journal of Materials Science: Materials in Electronics* (Submitted).
2. Sana Mehmood; Nadia Shahzad; **Saad Nadeem**; Muhammad Salik Qureshi; Abdul Sattar; Naseem Iqbal; Rabia Liaquat; Muhammad Imran Shahzad, “**Effect of lanthanum doped SnO_2 on the performance of mixed-cation mixed-halide perovskite for planar PSCs**”, *Thin Solid Films* (Submitted).
3. Muhammad Salik Qureshi; Nadia Shahzad; **Saad Nadeem**; Sana Mehmood; Abdul Sattar; Sehar Shakir; Muhammad Imran Shahzad, “**Study of Optical and electrical properties of SnO_2 - MoS_2 electron transport layer for perovskite solar cell**” (In Submission Process).

List of Abbreviations

ETL	Electron Transport Layer
HTL	Hole Transport Layer
PSCs	Perovskite solar cell
J _{sc}	Short circuit current density
V _{oc}	Open circuit voltage
FF	Fill-factor
PCE	Power conversion efficiency
ZTO	Zinc Tin Oxide
FA	Formamidinium
ZS	Zinc Stannate
MA	Methylammonium
FTO	Fluorine doped tin oxide
RT	Room temperature
TCO	Transparent conductive oxide
DMF	Dimethylformamide
DMSO	Dimethyl Sulfoxide
Ag	Silver
DSSCs	Dye sensitized solar cells
PCBM	Phenyl-C61-butyric acid methyl ester
BCP	Bathocuproine
PL	Photoluminescence
PSKT	Perovskite
Meso	Mesoporous
ITO	Indium tin oxide
Au	Gold

Chapter 1

Introduction

This chapter focuses on the introduction to the need for renewable sources of energy. Also, it sheds light on the effects of climate change in Pakistan and how using renewable energy sources, especially photovoltaics can prove fruit full in the longer run. Finally, the research objectives for the research on perovskite solar cells presented in this thesis are defined.

1.1 Fossil Fuels and Climate Change

Global warming and climate change are the biggest threats to the safe existence of humanity on the planet right now. Use of fossil fuels to power the world is the most relevant cause of ozone depletion, global warming, and unexpected climatic changes across the globe [1]. According to a report by International Energy Agency (IEA), more than 81% of the world's energy demand is filled by the consumption of fossil fuels [2]. And with the world's energy demand increasing with every passing year which in turn increases carbon emissions as depicted in a recent report by British petroleum [3]. This overwhelming use of fossil fuels badly impacts the air quality index across the globe in addition to global warming and ozone depletion [4]. Inhaling these pollutants can cause serious health issues which is why it is necessary to find alternative energy sources that are clean such as Wind, Solar, Tidal, Hydro, etc. Moreover, there is no endless supply of fossil fuels, World has already consumed more than 50% of its fossil fuel reserves [5], so it is essential to harvest from renewable energy sources for energy security for the coming generations.

1.2 Impacts of Climate Change in Pakistan

Pakistan is one of the most hardly hit countries by global warming and climate change. Rise in average temperature, un-predictable rain cycles leading to flooding, and very severe air quality index in big cities are the key highlights. All these issues are somewhat related to the use of fossil fuels in industry and transportation mainly. Global warming has hit Pakistan more severely as shown in a study by the world bank in Figure 1.1 [6]. A rise in average temperature is far more than predicted before. GHG emissions have also impacted agriculture and livestock in the country, moreover, a severe rise in average temperature and decrease in precipitation is expected by 2050.

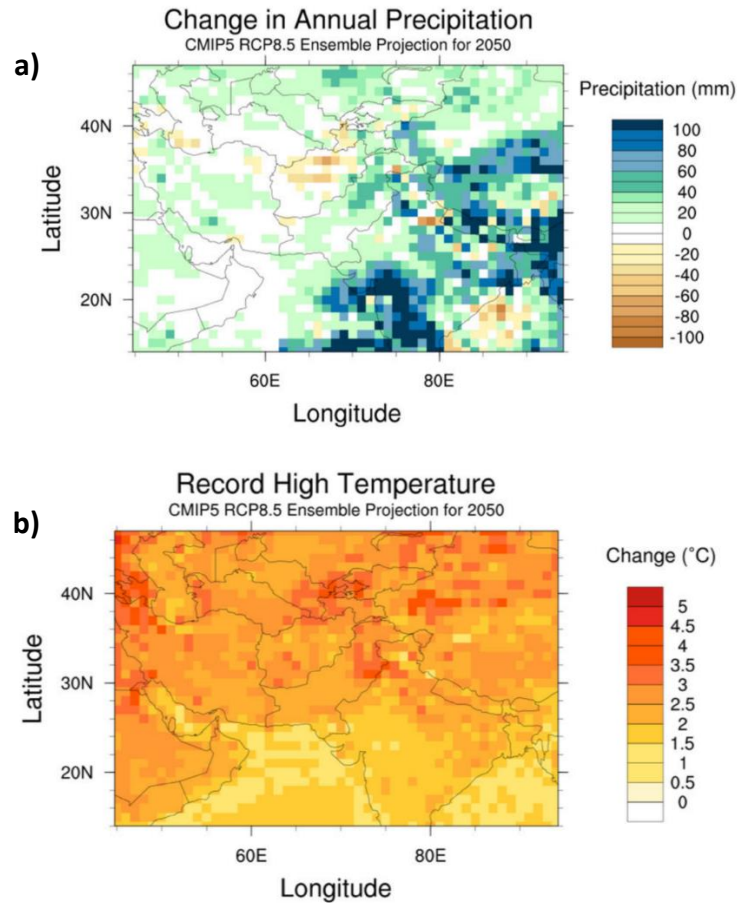


Figure 1.1 Projections for Pakistan (2050): a) Record high temperature, b) Impact on precipitation [7]

1.3 Renewable Energy: Potential and Policies in Pakistan

Pakistan has tremendous potential for solar, wind, and hydel energy. Most of the areas in the country have sunshine for 8 to 9 hours a day with a very high amount of solar insolation. One of the highest in the middle east as reported by IRENA [8]. The country is situated in one of the world’s highest solar energy potential areas [9].

Keeping these statistics in view, the country has a very ambitious renewable energy policy in place. With a target of reaching a 20% renewable share in the energy mix by 2025 and up to 30% by 2030, Pakistan needs to implement ground-breaking research and market incentives for the solar PV industry [10]. Pakistan is also a signatory of the Paris Agreement and Kyoto Protocol. To reach these goals the country needs indigenous development of solar panels. Recently the government has invested itself in solar net metering as photovoltaic-based net metering systems are gathering a lot of hype on the global spectrum due to obvious environmental and clean energy benefits. Net metering-

based solar PV technologies have generated 268 MW of electricity until now [9]. In order to further increase the photovoltaic-based energy in the country's energy mix government need to take steps in term of local manufacturing of solar panels. The work presented in this thesis is focused on the newest under research third generation of solar PV that may prove useful to fulfill Pakistan's local demand of PV technologies.

1.4 History of Solar PV Cells

Since the discovery of the photovoltaic effect in 1839 and the formation of the first silicon-based solar cell by Bell Labs in the 1950s for space applications silicon-based solar cells were fabricated commercially and were known as the first generation of PV cells which included the monocrystalline and polycrystalline solar cells [11]. The second generation of solar cells is also known as thin-film photovoltaics which includes devices based on CdTe and CIGS they are commercialized but struggle in competition with the first generation of solar cells [12], [13]. Then arrived the third generation of PV cells, this technology also brought the concept of tandem solar cells sandwiching the new perovskite-based cells with the first-generation silicon-based solar cells to enhance the device efficiency. The use of organic materials to harvest the solar irradiation of the sun resulted in the rise of a new generation of solar cells. It mainly includes four types of solar cell technologies [14].

- Dye-sensitized solar cells (DSSC).
- Perovskite solar cells (PSCs).
- Organic/Polymeric cells.
- Quantum dot solar cell.

Dye-sensitized solar cells (DSSCs) are from a group of thin-film solar cells that are under research from almost two decades due to their low cost, low temperature, and easy fabrication. Also, their development is environmentally friendly due to less toxic materials involved in their manufacturing. They consist of a Dye, electrode, counter electrode and an electrolyte that combine together to form a reversible reaction [15]. Perovskite solar cells (PSCs) are considered as an improved form of DSSCs as they were discovered after the dye-based solar cells. They consist of an Electron transport layer (ETL), Hole transport layer (HTL), and a perovskite absorber layer respectively. Various structures and

configurations are reported for these solar cells [16]. The polymeric solar cells consist of a layered structure that consist of a semiconductor material (polymeric), a transparent front electrode for sunlight to transmit, and back electrode mostly printed on a plastic substrate respectively. The polymeric semiconductor material acts as a photoactive material in this setup [17]. A quantum dot solar cell (QDSC) uses quantum dots as photoactive material to replace the bulky materials such as silicon, or copper indium gallium selenide. Quantum dot solar cells offer better band gap control as it is tunable by changing the size of these atomic quantum dots respectively [18]. This generation of solar cells offers cheap fabrication costs and more flexibility in application. Whereas the traditional silicon-based solar cells usually are costly and difficult to fabricate due to the requirement of high processing temperature due to the involvement of silicon [19]. But this generation of solar cells is still facing problems in ambient stability that are keeping it from being commercialized. Currently, an efficiency of 25.8% is achieved for PSC and 33.2% for perovskite tandem solar cells [20].

1.5 Perovskite Solar Cells (PSCs)

1.5.1 Working Principle

The working principle of a perovskite solar cell is different from the traditional silicon-based solar cells. As separate hole and electron extraction layers are combined with a separate light absorption perovskite layer. Whereas in the case of silicon there is a p and n-type layer that functions as charge generation and extraction layers. In the case of perovskite solar cells, sunlight is absorbed by the perovskite layer that in turn generates electron-hole pairs. These electrons and holes are then transported out of the perovskite layer by hole and electron transport layers. The charge is then transported to the external circuit through metallic and transparent electrodes as shown in Figure 1.2 [21]. Here it is very important to consider the valence and conduction band alignment of different layers. Because all the charge flow in perovskite solar cells is based on band alignment. HTL and ETL act to perform their corresponding charge transport functionalities as well as for blocking the reverse flow of charge which can result in recombination and consequently very low efficiency.

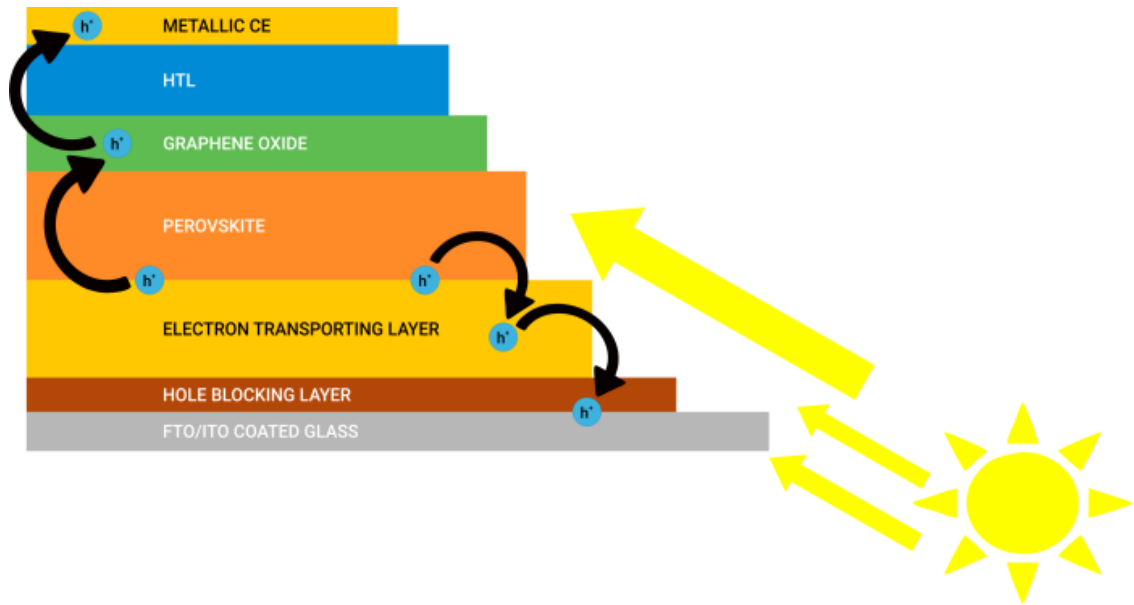


Figure 1.2 Working principle of perovskite solar cell (PSC) [21]

1.5.2 Device Architecture

There are two main types of planar cell architectures being employed in perovskite solar cells inverted planar (p-i-n) and planar (n-i-p), as shown in Figure 1.3. Both consist of an Absorber layer, hole transport layer (HTL), Electron transport layer, and TCO [22]. In the p-i-n architecture (also known as an inverted architecture) the hole transport layer is deposited first followed by the absorber layer and the electron transport layer respectively as shown in the Figure 1.3b. This type of architecture offers low temperature manufacturing and limited hysteresis in the developed devices. The n-i-p mesoscopic structure was one of the very first device structures that was tested as a perovskite solar cell. Later a solid hole transport layer was added in place of mesoscopic structure to improve the charge transport characteristics. To make a device following this structure an electron transport layer is first deposited on a FTO and is followed by an absorber layer and a hole transport layer as shown in Figure 1.3a respectively. This structure shows a great V_{oc} and J_{sc} but also reports of high hysteresis loss are evident from the literature.

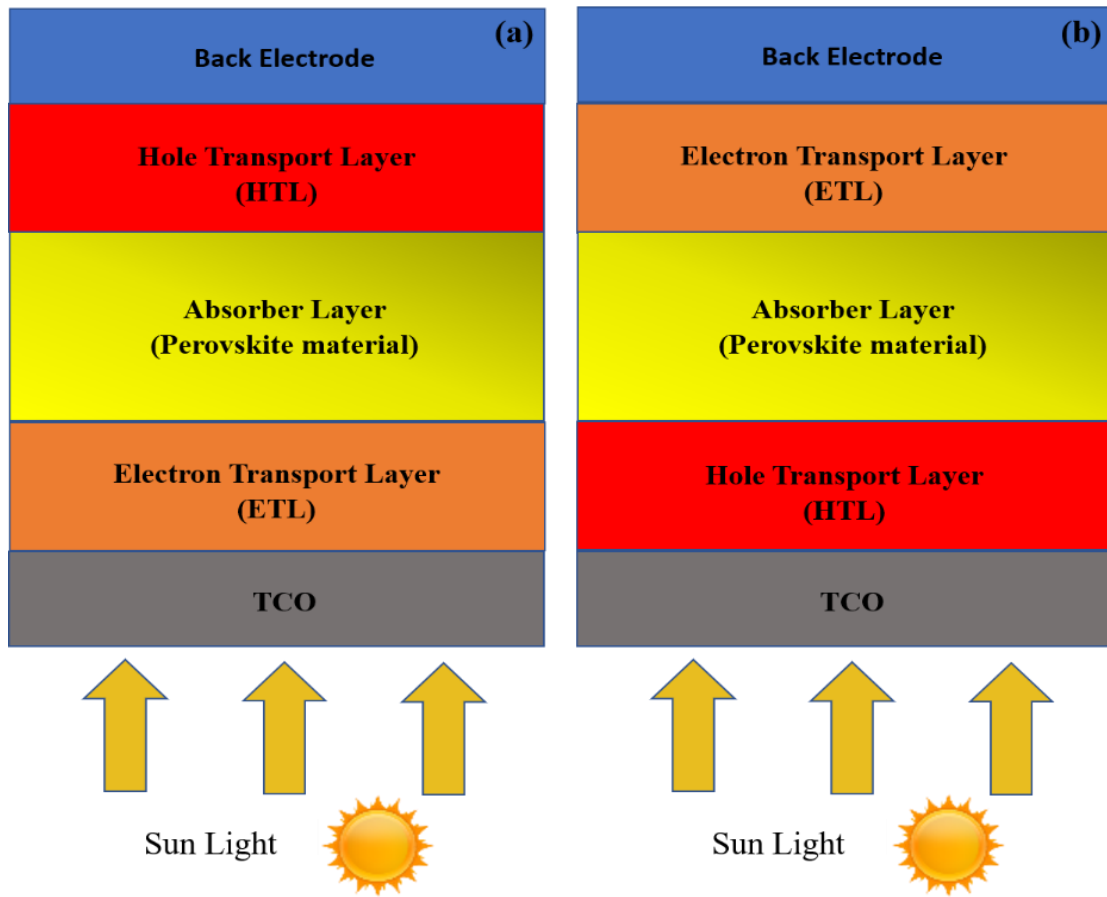


Figure 1.3 Different structures of a PSC: (a) Planar (n-i-p), (b) inverted planar (p-i-n) [22]

1.6 Electron Transport Layers (ETLs)

The electron transport layer (ETL) is a crucial component of perovskite solar cells, playing a vital role in the overall efficiency and performance of the device by facilitating the efficient extraction and transport of electrons generated in the active perovskite layer to the corresponding electrode [23]. To function effectively, ETLs must possess several key characteristics. They should have high electron mobility to ensure rapid and efficient electron transport. The energy levels of the ETL should align well with the perovskite layer to facilitate efficient charge transfer and minimize potential barriers for electron transport. ETLs should selectively transport electrons while blocking holes, ensuring efficient charge separation. Furthermore, ETLs should exhibit chemical and environmental stability under various conditions, including humidity, temperature, and light exposure, to guarantee the long-term performance and stability of the solar cell.

1.6.1 Role Of ETLs in Perovskite Solar Cells

In perovskite solar cells, the ETL plays several essential roles. Firstly, it selectively transports electrons from the perovskite layer to the electrode while blocking the flow of holes, ensuring efficient charge separation. Secondly, by efficiently extracting electrons, the ETL helps suppress charge recombination between electrons and holes, which can lead to energy loss and reduced device performance [24]. Lastly, a high-quality ETL can help passivate the perovskite surface, reducing surface defects and improving device stability over time.

1.6.2 Types of Electron Transport Layers

There are two primary types of electron transport layers based on their composition: binary and ternary. Binary ETLs are composed of a single material, typically an inorganic metal oxide or an organic semiconductor. Common examples include TiO_2 (Titanium dioxide), SnO_2 (Tin dioxide), and ZnO (Zinc oxide) [25], [26]. These materials often exhibit desirable characteristics such as high electron mobility, suitable energy band alignment, and excellent stability. On the other hand, ternary ETLs are composed of a mixture of two or more materials, which can lead to synergistic effects and improved performance. Examples of ternary ETLs include TiO_2/ZnO , $\text{TiO}_2/\text{Graphene}$, and $\text{SnO}_2/\text{C60}$ composites [27], [28]. By combining the unique properties of multiple materials, ternary ETLs can exhibit enhanced performance characteristics, such as improved electron mobility, better charge selectivity, and increased stability.

1.7 Problem Statement

Despite the current dominance of binary metal oxides in electron transport materials for PSCs, there are still some deficiencies like low electron mobility and high trap state density in TiO_2 and poor chemical stability in ZnO , prompting the search for alternative options such as ternary metal oxides. Within ternary metal oxides, bilayers comprising both crystalline and amorphous forms of ternary metal oxides represent a relatively untapped area of research in the development of ETLs for PSCs, offering a myriad of possibilities for further study.

1.8 Research Objectives

In order to address the research question and achieve the aims of this study, the following research objectives had been established:

- Fabrication of ternary metal oxides-based electron transport layer for perovskite solar cells (PSCs).
- Optical and electrical properties, characterization and morphological analysis of ternary metal oxide-based electron transport layer.
- Optimization and suitability of the prepared electron transport layer for perovskite solar cell.

Summary

This chapter develops the context for the need of solar photovoltaic technology highlighting the current crises of climate change originating from the excessive use of fossil fuels as the available source of energy. Moreover, it also discusses the impact of fossil fuels consumption on the entire ecosystem and particularly on human health. Then, it states the role of renewable energy to mitigate climatic change effects and the bright future of solar photovoltaic technology as a leader to bring this change. Further, it states the different generations of the photovoltaic solar cells and the progress of PSC devices as well as the device architectures. The chapter also covers the characteristics of an efficient electron transport layer (ETLs) and its role in perovskite solar cells (PSCs). Subsequently, the discussion encompasses the problem statement and delineates the objectives of this research work.

References

- [1] K. Annamalai, S. S. Thanapal, and D. Ranjan, “Ranking Renewable and Fossil Fuels on Global Warming Potential Using Respiratory Quotient Concept,” *J. Combust.*, vol. 2018, 2018, doi: 10.1155/2018/1270708.
- [2] “World Energy Balances - Data product - IEA.” <https://www.iea.org/data-and-statistics/data-product/world-energy-balances#world> (accessed May 01, 2023).
- [3] “Statistical Review of World Energy | Energy economics | Home.” <https://www.bp.com/en/global/corporate/energy-economics/statistical-review-of-world-energy.html> (accessed May 01, 2023).
- [4] F. Martins, C. Felgueiras, M. Smitkova, and N. Caetano, “Analysis of fossil fuel energy consumption and environmental impacts in european countries,” *Energies*, vol. 12, no. 6, pp. 1–11, 2019, doi: 10.3390/en12060964.
- [5] M. Höök and X. Tang, “Depletion of fossil fuels and anthropogenic climate change- A review,” *Energy Policy*, vol. 52, pp. 797–809, 2013, doi: 10.1016/j.enpol.2012.10.046.
- [6] “Pakistan - Climatology | Climate Change Knowledge Portal.” <https://climateknowledgeportal.worldbank.org/country/pakistan/climate-data-historical> (accessed May 01, 2023).
- [7] M. Hussain *et al.*, “A comprehensive review of climate change impacts, adaptation, and mitigation on environmental and natural calamities in Pakistan,” *Environ. Monit. Assess.*, vol. 192, no. 1, 2020, doi: 10.1007/s10661-019-7956-4.
- [8] IRENA, *Renewables Readiness Assessment: Pakistan*, International Renewable Energy Agency (IRENA), Abu Dhabi., no. November. 2018.
- [9] “Assessment of Net-Metering Based Solar Systems installed at IESCO & LESCO - Institute of Policy Studies.” <https://www.ips.org.pk/assessment-of-net-metering-based-solar-systems-installed-at-iesco-lesco/> (accessed May 01, 2023).

- [10] “Variable Renewable Energy Integration and Planning Study,” *Var. Renew. Energy Integr. Plan. Study*, 2020, doi: 10.1596/34586.
- [11] Allen, T.G., Bullock, J., Yang, X. et al. "Passivating contacts for crystalline silicon solar cells". *Nat Energy* 4, 914–928 (2019). [Online]. Available: <http://dx.doi.org/10.1038/s41560-019-0463-6>.
- [12] S. C. Bhatia, “Solar devices,” *Adv. Renew. Energy Syst.*, pp. 68–93, Jan. 2014, doi: 10.1016/B978-1-78242-269-3.50003-6.
- [13] O. K. Simya, P. Radhakrishnan, A. Ashok, K. Kavitha, and R. Althaf, “Engineered nanomaterials for energy applications,” *Handb. Nanomater. Ind. Appl.*, pp. 751–767, 2018, doi: 10.1016/B978-0-12-813351-4.00043-2.
- [14] J. Yan and B. R. Saunders, “Third-generation solar cells: A review and comparison of polymer:fullerene, hybrid polymer and perovskite solar cells,” *RSC Adv.*, vol. 4, no. 82, pp. 43286–43314, 2014, doi: 10.1039/c4ra07064j.
- [15] K. Sharma, V. Sharma, and S. S. Sharma, “Dye-Sensitized Solar Cells: Fundamentals and Current Status,” *Nanoscale Res. Lett.*, vol. 13, 2018, doi: 10.1186/s11671-018-2760-6.
- [16] U. Krishnan, “Factors affecting the stability of perovskite solar cells: a comprehensive review,” *J. Photonics Energy*, vol. 9, no. 02, p. 1, 2019, doi: 10.1117/1.jpe.9.021001.
- [17] M. R. Geiker and M. M. Andersen, “Nanotechnologies for sustainable construction,” *Sustain. Constr. Mater.*, pp. 254–283, 2009, doi: 10.1533/9781845695842.254.
- [18] “Quantum Dot Solar Cells Are Coming | AltEnergyMag.” <https://www.altenergymag.com/article/2018/05/quantum-dot-solar-cells-are-coming/28547> (accessed May 01, 2023).
- [19] M. Cai, Y. Wu, H. Chen, X. Yang, Y. Qiang, and L. Han, “Cost-Performance Analysis of Perovskite Solar Modules,” *Adv. Sci.*, vol. 4, no. 1, 2017, doi: 10.1002/advs.201600269.

- [20] “Best Research-Cell Efficiency Chart | Photovoltaic Research | NREL.” <https://www.nrel.gov/pv/cell-efficiency.html> (accessed May 01, 2023).
- [21] I. Mora-Seró, “How Do Perovskite Solar Cells Work?,” *Joule*, vol. 2, no. 4, pp. 585–587, 2018, doi: 10.1016/j.joule.2018.03.020.
- [22] I. Hussain, H. P. Tran, J. Jaksik, J. Moore, N. Islam, and M. J. Uddin, “Functional materials, device architecture, and flexibility of perovskite solar cell,” *Emergent Mater.*, vol. 1, no. 3–4, pp. 133–154, 2018, doi: 10.1007/s42247-018-0013-1.
- [23] J. P. Correa-Baena *et al.*, “Promises and challenges of perovskite solar cells,” *Science (80-.86)*, vol. 358, no. 6364, pp. 739–744, 2017, doi: 10.1126/science.aam6323.
- [24] S. D. Stranks *et al.*, “Electron-hole diffusion lengths exceeding 1 micrometer in an organometal trihalide perovskite absorber,” *Science (80-.84)*, vol. 342, no. 6156, pp. 341–344, 2013, doi: 10.1126/science.1243982.
- [25] A. Hagfeldt, G. Boschloo, L. Sun, L. Kloo, and H. Pettersson, “Dye-Sensitized Solar Cells,” pp. 6595–6663, 2010.
- [26] W. Ke *et al.*, “Lowerature solution-processed tin oxide as an alternative electron transporting layer for efficient perovskite solar cells,” *J. Am. Chem. Soc.*, vol. 137, no. 21, pp. 6730–6733, 2015, doi: 10.1021/jacs.5b01994.
- [27] M. Anaya, G. Lozano, M. E. Calvo, and H. Míguez, “ABX3 Perovskites for Tandem Solar Cells,” *Joule*, vol. 1, no. 4, pp. 769–793, 2017, doi: 10.1016/j.joule.2017.09.017.
- [28] Z. Zhu *et al.*, “High-performance hole-extraction layer of sol-gel-processed nio nanocrystals for inverted planar perovskite solar cells,” *Angew. Chemie - Int. Ed.*, vol. 53, no. 46, pp. 12571–12575, 2014, doi: 10.1002/anie.201405176.

Chapter 2

Literature Review

Perovskite solar cells have emerged as a promising photovoltaic technology due to their exceptional power conversion efficiency (PCE) and cost-effective fabrication processes. One of the critical components in perovskite solar cells is the electron transport layer (ETL), which plays a pivotal role in facilitating efficient charge separation, electron extraction, and preventing recombination. The choice of ETL material and its interface with the perovskite layer significantly influence the overall performance, stability, and durability of the solar cell. This literature review aims to provide an in-depth analysis of the various aspects of electron transport layers in perovskite solar cells, including the fundamental properties, commonly used materials (including both binary and ternary metal oxide ETLs) and fabrication techniques. Furthermore, the chapter reflects on the progress made in the research and development of ETLs for perovskite solar cells, highlighting the milestones and breakthroughs that have shaped this rapidly evolving field.

2.1 Characteristics of Metal Oxide Electron Transport Layers

Attaining a high-power conversion efficiency (PCE) in perovskite solar cells (PSCs) necessitates the efficient separation of photogenerated charges and minimization of nonradiative recombination. The electron transport layer (ETL) serves a crucial function in extracting and transporting photogenerated electrons while also preventing hole conduction, thereby reducing charge recombination. Consequently, the photovoltaic performance of PSCs is heavily influenced by the properties of ETLs, particularly their electronic characteristics (energy levels, mobility, trap states), optical features (bandgap, refractive index), morphological control, and chemical stability with respect to the adjacent perovskite absorber layer.

2.1.1 Electronic Properties

The electronic properties of electron transport layers (ETLs) play a critical role in determining the performance of perovskite solar cells (PSCs). Key electronic properties include energy level alignment, electron mobility, and trap states, as shown in Figure 2.1a, b. In this section, we discuss these properties and their impact on PSCs' overall efficiency.

The alignment of energy levels between the ETL and the perovskite absorber is crucial for efficient charge extraction and minimizing recombination at the interface [1]. An ideal ETL should possess a conduction band edge that aligns well with the perovskite layer's conduction band edge, allowing for seamless electron transfer [2]. This energy level alignment can also influence the open-circuit voltage (V_{oc}) and the fill factor (FF) of the device [3]. High electron mobility in ETLs is essential for rapid electron transport and reduced recombination losses, which in turn improves the overall device performance [4]. A high electron mobility material reduces the chances of electron-hole recombination within the ETL or at the perovskite/ETL interface, ultimately leading to enhanced photocurrent and PCE [5]. Trap states in ETL materials can lead to increased charge recombination, reduced carrier lifetime, and diminished overall device performance [6]. It is therefore vital to minimize the trap density in ETL materials through material engineering, doping, or surface passivation techniques [7].

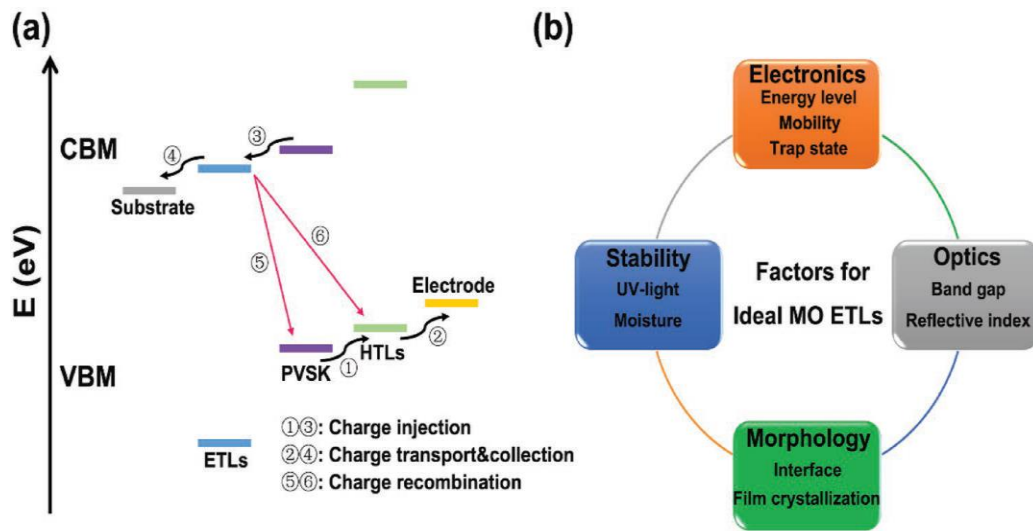


Figure 2.1 a) Schematic diagram of carrier injection and collection in PSCs. b) Important factors for ideal electron transport layers

2.1.2 Optical Properties

The optical properties of electron transport layers (ETLs) in perovskite solar cells (PSCs) significantly impact the overall device performance. In this section, we discuss two key optical properties—bandgap and refractive index—and their implications for PSCs.

The bandgap of ETL materials plays a vital role in determining the device's overall light absorption and photocurrent generation [8]. An ideal ETL should have a wide bandgap to

ensure minimal absorption of incident light, allowing for more efficient light penetration and absorption by the perovskite absorber layer [9]. A wide bandgap ETL also ensures proper energy level alignment between the ETL and perovskite layer, facilitating efficient electron transfer and reducing recombination [10]. The refractive index of ETL materials influences light trapping and scattering within the solar cell, which in turn affects the overall light absorption and device performance [11]. A lower refractive index ETL can enhance light management in PSCs by minimizing reflection losses and maximizing light coupling into the perovskite layer [12]. Additionally, tailoring the refractive index of the ETL can help optimize the device's optical properties for specific wavelength ranges, leading to improved performance [13].

2.1.3 Morphology Control

Controlling the morphology of electron transport layers (ETLs) is crucial for achieving high-performance perovskite solar cells (PSCs). This section discusses two key aspects of morphology control—interface engineering and film crystallization—and their implications for PSCs.

The ETL-perovskite interface plays a significant role in determining the overall device performance, with factors such as surface roughness, uniformity, and coverage affecting charge transfer and recombination [14]. A well-engineered interface with a smooth, conformal ETL layer can minimize charge recombination and enhance the efficiency of electron extraction [15]. Various strategies have been developed to optimize the ETL-perovskite interface, including solvent engineering, self-assembly monolayers, and deposition of ultrathin interlayers [16], [17]. The crystallinity and grain structure of ETL films can also influence the photovoltaic performance of PSCs. High-quality ETL films with large grains and low defect densities can facilitate efficient electron transport, reduce charge recombination, and improve device stability [18]. Various deposition techniques and post-treatment methods, such as annealing and solvent vapor treatment, have been explored to control the crystallization and grain growth of ETL films [19].

2.1.4 Chemical Stability

The chemical stability of electron transport layers (ETLs) is critical for the long-term performance and durability of perovskite solar cells (PSCs).

Prolonged exposure to UV light can degrade ETL materials, leading to reduced device performance and stability [20]. UV-induced degradation can result in the formation of defects, increased recombination, and reduced electron mobility in ETLs [21]. To improve the UV stability of ETLs, various strategies have been employed, such as incorporating UV-absorbing materials, utilizing wide bandgap materials, and applying protective layers or coatings [22], [23]. Moisture-induced degradation is another significant challenge for the stability of ETLs in PSCs, as the ingress of water or moisture can cause material degradation, delamination, and increased recombination [24]. Various approaches have been developed to enhance the moisture stability of ETLs, including the use of hydrophobic materials, encapsulation techniques, and surface modification methods [25], [26].

2.2 Binary and Ternary Metal Oxide Electron Transport Layers

To optimize the performance of PSCs, various ETL materials have been explored, including binary and ternary metal oxides. Binary metal oxide ETLs, such as TiO_2 and SnO_2 , have been widely investigated owing to their favorable electronic and optical properties. However, ternary metal oxide ETLs, including Zn_2SnO_4 and BaSnO_3 , have recently emerged as promising alternatives due to their enhanced stability, tunable band structure, and improved charge transport properties [27], [28]. This section aims to provide a comprehensive overview of the recent advances in binary and ternary metal oxide ETLs for perovskite solar cells, examining their electronic, optical, and morphological properties, as well as their impact on device performance and stability.

2.2.1 Binary Metal Oxide ETLs

Binary metal oxide electron transport layers (ETLs) have been widely studied for their role in enhancing the performance of perovskite solar cells (PSCs). Titanium dioxide (TiO_2) is a well-known ETL material for PSCs due to its high electron mobility, wide bandgap, and suitable energy level alignment with perovskite absorbers. Kojima et. al were the first to utilize commercial nanocrystalline TiO_2 paste to create a mesoporous ETL, which served as both a support layer and charge extraction layer [29]. Mei et. al reported a fully printable, hole-transport-layer-free carbon electrode-based PSC using screen-printed TiO_2 as a mesoporous ETL and scaffold [30]. For planar PSCs, Liu et. al employed

a compact TiO_2 layer as the ETL, achieving a power conversion efficiency (PCE) of 15.4% [18]. Similarly, Li et. al, as well as Wang and colleagues, employed a high-temperature-processed SnO_2 layer as the compact layer and used SnO_2 and TiO_2 nanoparticles as mesoporous layers for PSCs. As a result, they achieved power conversion efficiencies of 6.5% and 7.4%, respectively [25], [31]. Lai et al. employed radio frequency (RF) sputtered ZnO as the electron transport layer in inverted perovskite solar cells, achieving a power conversion efficiency of 10.9% [32]. Wang et al. successfully employed low-temperature-processed CeO_x as ETLs in high-performance PSCs, achieving a power conversion efficiency of 14.32% [33].

2.2.2 Ternary Metal Oxide ETLs

In comparison to the more common binary oxides, ternary oxides provide an increased level of flexibility, making it possible to fine-tune various aspects of ternary metal oxide materials through simple adjustments in their chemical composition [34]. Ternary metal oxides have recently attracted a lot of attention as effective electron transport layers (ETLs). For instance, Ye et al. incorporated NaTaO_3 ternary metal oxide ETL in PSCs and reported an efficiency of 21.07% with improved device stability [35]. Li and his team explored the potential of ternary metal oxides based on Ti-Fe-O as efficient ETLs, discovering a decrease in surface recombination and favorable charge collection characteristics in which the perovskite device utilizing $\text{Ti}_{0.5}\text{Fe}_{0.5}\text{O}_x$ attained the maximum power conversion efficiency (PCE) of 14.7% [36]. Similarly, Wei's group reported the PCE of 19.8% when ZnTiO_3 ternary metal oxide ETL was incorporated in PSCs [37]. Among a range of ternary metal oxides, zinc-tin based ETLs demonstrate significant potential in perovskite solar cell applications. Zinc-tin based ternary oxides exhibit a broader band-gap, high electron mobility, and a low refractive index with high chemical stability. For example, Oh et al. reported an improved electron diffusion and superior charge collection with Zinc Stannate (Zn_2SnO_4) ETL in PSCs as compared to the conventional TiO_2 with similar device performance [27]. Thambidurai et al. studied the viability of various zinc-tin-oxides (ZTO) as potential ETL alternative in PSCs, discovering that the device with $\text{Zn}_1\text{Sn}_1\text{O}_x/\text{SnO}_2$ as a bilayer ETL achieved the maximum PCE of 19.01% exhibiting enhanced charge collection and decreased charge recombination [38]. Furthermore, Shalan et al. showed that ZTO ETLs yielded better

photovoltaic properties, attaining a peak power conversion efficiency (PCE) of 17.81%, in contrast with ZnO binary metal oxide ETLs with PCE of 12.02% [39].

2.3 Bi-Layer Metal Oxide Electron Transport Layers

Bilayer electron transport layers (ETLs) have emerged as a promising approach to enhancing the efficiency and stability of perovskite solar cells (PSCs). These innovative structures comprise two distinct functional layers, carefully engineered to optimize charge separation and transport. By tailoring the properties of each layer to the specific requirements of the perovskite material, researchers have been able to minimize recombination losses and improve overall device performance. In order to provide a more comprehensive understanding of the bilayer ETLs utilized in perovskite solar cells, we present Table 1, which contains a selection of notable examples along with their corresponding photovoltaic properties. This table showcases the diversity in material selection and layer configurations, demonstrating the versatility of bilayer ETLs in achieving improved photovoltaic performance.

2.3.1 Deposition Methods of Metal Oxide Electron Transport Layers

The deposition of electron transport layers (ETLs) plays a crucial role in determining the efficiency and stability of perovskite solar cells (PSCs). Various techniques have been developed to deposit ETLs, each offering unique advantages and challenges. The choice of deposition method significantly impacts the morphological, electrical, and optical properties of the ETL, ultimately affecting the overall performance of the solar cell. This section provides an overview of the primary deposition methods employed for ETLs in perovskite solar cells.

2.3.1.1 Solution Process Method

The solution process method has become a widely-used technique for the deposition of electron transport layers (ETLs) in perovskite solar cells (PSCs) due to its simplicity, cost-effectiveness, and compatibility with various materials [40]. The choice of solvent and precursor materials is crucial in the solution process method. Researchers have explored various solvents, such as ethanol, isopropanol, and chlorobenzene, to optimize the ETL film quality [41]. The use of additives, such as hydroiodic acid, has also been reported to improve the morphology and conductivity of the ETL [3].

Table 1 Photovoltaic performances of PSC devices with multi-layer ETLs

ETLs	Device Structure	V_{oc} (V)	J_{sc} (mA/cm²)	FF	PCE (%)	Ref.
TiO ₂ / WO ₃	FTO / TiO ₂ / WO ₃ / perovskite / Spiro-OMeTAD / Ag	1.09	23.54	0.79	20.14	[42]
ZnO / SnO ₂	ITO / ZnO / SnO ₂ / perovskite / Spiro-OMeTAD / Ag	1.15	21.74	0.76	19.10	[43]
ZnO / Zn ₂ SnO ₄	FTO / ZnO / ZTO / PCBM / Perovskite / Spiro-OMeTAD / Au	1.07	23.20	0.74	18.30	[44]
Nb ₂ O ₅ / TiO ₂	FTO / Nb ₂ O ₅ -TiO ₂ / Perovskite / Spiro-OMeTAD / Au	1.04	20.49	0.72	15.25	[45]
WO _x / SnO ₂	ITO / WO _x / SnO ₂ / Perovskite / Spiro-OMeTAD / Ag	1.11	23.01	0.80	20.52	[46]
ZnO / CeO _x	FTO / ZnO / CeO _x / Perovskite / Spiro-OMeTAD / Au	1.09	23.64	0.76	19.52	[47]
PCBM / ZnO	ITO / NiO / Perovskite / PCBM / ZnO / Cu	1.06	22.98	0.80	19.36	[48]
C ₆₀ / BCP	ITO / NiO / Perovskite / C ₆₀ / BCP / Cu	1.02	22.12	0.77	17.10	[48]
TiO ₂ / SnO ₂	FTO / TiO ₂ / SnO ₂ / perovskite / Spiro-OMeTAD / Au	1.00	22.73	0.67	15.29	[49]

ETLs	Device Structure	Voc (V)	Jsc (mA/cm²)	FF	PCE (%)	Ref.
TiO ₂ / AZO	FTO / TiO ₂ / AZO / perovskite / Spiro-OMeTAD / Au	1.05	19.49	0.68	13.94	[50]
SnO ₂ / ZnO	ITO / SnO ₂ / ZnO / AZO / perovskite / Spiro-OMeTAD / Au	1.20	22.10	0.77	20.43	[51]
IL / Nb ₂ O ₅	FTO / IL / Nb ₂ O ₅ / perovskite / Spiro-OMeTAD / Au	1.05	22.20	0.70	16.40	[52]
PCBM / Nb ₂ O ₅	FTO / PCBM / Nb ₂ O ₅ / perovskite / Spiro-OMeTAD / Au	1.09	21.00	0.73	16.60	[52]
Sn:In ₂ O ₃ / In ₂ O ₃	ITO / NiO / Perovskite / Sn:In ₂ O ₃ / In ₂ O ₃ / Ag	1.10	23.22	0.81	20.65	[53]

One challenge of the solution process method is the potential for inhomogeneous films, which can lead to performance losses due to increased recombination [54]. To overcome this issue, researchers have investigated the use of two-dimensional (2D) materials, such as graphene and transition metal dichalcogenides, as additives to improve the uniformity and conductivity of the ETL [55].

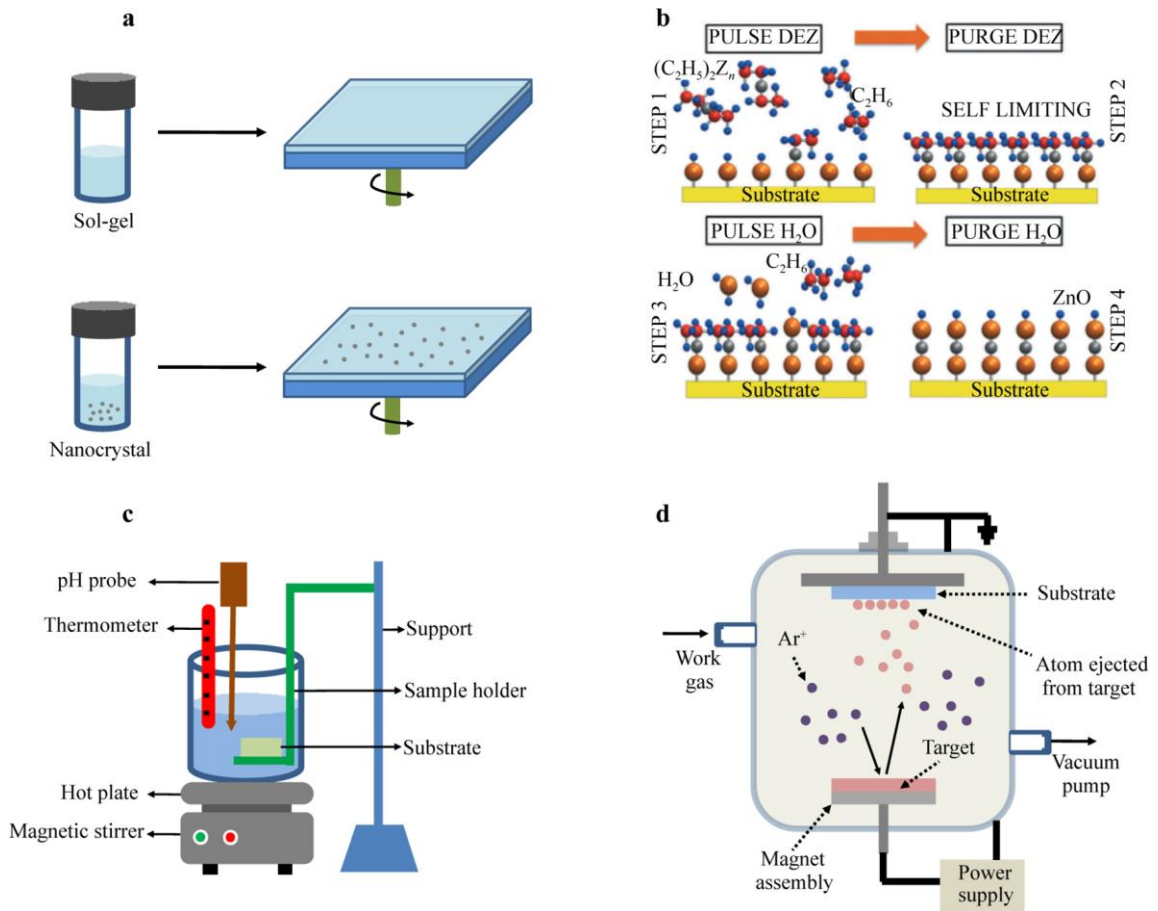


Figure 2.2 Depiction of common techniques for depositing MO ETLs: a) solution process b) atomic layer deposition c) chemical bath deposition and d) magnetron sputtering

2.3.1.2 Atomic Layer Deposition

Atomic layer deposition (ALD) has emerged as a promising technique for the deposition of electron transport layers (ETLs) in perovskite solar cells (PSCs), due to its precise control over film thickness, excellent conformality, and ability to produce highly uniform layers [56][57].

ALD has been used to deposit various materials as ETLs in PSCs, including metal oxides such as TiO_2 , SnO_2 , and ZnO [58], [59][60]. The ultra-thin, conformal nature of ALD films has been shown to enhance the charge extraction and transport properties of ETLs, ultimately leading to improved device performance. However, the ALD process is relatively slow and more expensive than solution-based methods, which may limit its widespread adoption in large-scale PSC production [61].

2.3.1.3 Chemical Bath Deposition

Chemical bath deposition (CBD) has been recognized as a cost-effective and straightforward technique for the deposition of electron transport layers (ETLs) in perovskite solar cells (PSCs). This method involves immersing a substrate in a chemical solution containing precursors, which react to form a thin film on the surface. One of the most common materials deposited using CBD for PSCs is CdS , which has been reported to yield improved photovoltaic performance when used as an ETL [62]. Furthermore, CBD has been utilized to deposit other materials, such as In_2S_3 and ZnO , as ETLs in PSCs [63], [64].

A major advantage of CBD is its low cost and simplicity, making it particularly attractive for large-scale production of PSCs. Additionally, it enables the deposition of films at low temperatures, which is suitable for temperature-sensitive perovskite materials [65].

2.3.1.4 Other Deposition Methods

A variety of deposition techniques have been employed for the fabrication of electron transport layers (ETLs) in perovskite solar cells (PSCs), each with its unique advantages and limitations. Electrochemical deposition, also known as electrodeposition, is a versatile technique used to deposit ETLs in PSCs. This method involves the reduction of metal ions at a cathode through the application of an electric potential. The method offers advantages such as low cost, good film uniformity, and precise control over film thickness [66]. However, the technique may require the use of a conductive substrate, which could limit its application in PSCs. Moreover, Magnetron sputtering is another deposition technique. It is a physical vapor deposition technique that has been used to deposit various ETL materials, including TiO_2 , ZnO , and SnO_2 , in PSCs [67], [68]. The method involves the use of a magnetron to eject atoms from a target material, which then condense onto a

substrate. This technique is known for producing high-quality, dense, and uniform films with good control over thickness and morphology [69]. Electron-beam (e-beam) deposition is another physical vapor deposition technique used for depositing ETLs in PSCs. This method utilizes a high-energy electron beam to evaporate target materials, which then condense on a substrate. The technique is known for producing high-quality films with excellent control over thickness and composition. Additionally, e-beam deposition can achieve high deposition rates and uniformity [70]. However, the high equipment cost and complexity of the process may limit its application in large-scale PSC production.

2.4 Evolution of Bilayer Ternary Metal Oxide ETLs

The bilayer ternary metal oxide-based ETL was proposed as an alternative in the mid-2010s. This concept combined two different metal oxides, such as $\text{Zn}_2\text{SnO}_4/\text{SnO}_2$ and TiO_2/ZnO [71], [72]. The aim was to harness the advantages of each component while minimizing their drawbacks, such as improving UV stability and reducing the processing temperature. The efficiency of PSCs with bilayer ternary metal oxide-based ETLs has seen significant improvements over the years. Several strategies have been employed to achieve this, including material engineering, interface modification, and doping techniques [73],[74], [75]. Material engineering, such as altering the stoichiometry of the metal oxides, has led to enhanced electronic properties and improved energy level alignment with perovskite materials [76].

2.4.1 Unexplored Avenues in Research

Bilayers comprising both crystalline and amorphous forms of ternary metal oxides represent a relatively untapped area of research in the development of Electron Transport Layers (ETLs) for perovskite solar cells. The unique combination of the two forms of metal oxides - one amorphous and one crystalline - offers a myriad of possibilities for further study. The structural characteristics of these materials, including their morphology and crystallinity, could be manipulated to provide significant advantages for ETL performance. Additionally, the investigation of the hydrophobic or hydrophilic nature of these layers is of great interest. The water interaction properties of the ETL can profoundly impact the stability and longevity of perovskite solar cells, especially considering the

known sensitivity of perovskite materials to moisture. If these bilayers can be engineered to have specific water interaction properties, they might be used to improve the environmental robustness of perovskite solar cells.

2.4.2 Proposed Action Plan

In this research, a solution-based technique is employed to produce dense and uniform thin films of zinc stannate (ZS) and zinc-tin oxide (ZTO), as well as their bilayer, presenting a potential ETL choice for high performance and efficient planar PSCs. The opto-electronic properties of these materials were examined, along with their morphological analysis and compatibility with cesium-doped methylammonium lead iodide perovskite layer $\text{Cs}_{0.1}\text{MA}_{0.9}\text{Pb}(\text{I}_{0.9}\text{Br}_{0.1})_3$. Essentially, the study highlights the potential of zinc-tin based ternary metal oxides as a superior ETL alternative due to their exceptional intrinsic properties. Furthermore, improvement in photovoltaic parameters such as charge carrier mobility, surface morphology and reduced carrier recombination were demonstrated using the ZS/ZTO bilayer ETL.

Summary

The study of metal oxide electron transport layers (ETLs) for perovskite solar cells involves examining their electronic and optical properties, morphology control, and chemical stability. Researchers have explored both binary and ternary metal oxide ETLs, as well as bi-layer metal oxide ETLs, to optimize device performance. The deposition of electron transport layers (ETLs) is crucial for the efficiency and stability of perovskite solar cells (PSCs), and various techniques have been developed to address this need. These methods include the solution process method, which is popular for its simplicity and cost-effectiveness; atomic layer deposition (ALD), known for its precise control over film thickness and uniformity; chemical bath deposition (CBD), which is cost-effective and straightforward; and other techniques like electrochemical deposition, magnetron sputtering, and electron-beam deposition, each offering unique advantages and limitations. The choice of deposition method has a significant impact on the morphological, electrical, and optical properties of the ETL, ultimately affecting the solar cell's performance. Introduced in the mid-2010s, bilayer ternary metal oxide-based Electron Transport Layers (ETLs) have significantly improved perovskite solar cell efficiency through material engineering, interface modification, and doping techniques. However, the potential of crystalline and amorphous bilayers remains largely untapped, particularly in terms of their morphological, structural, and hydrophilic/hydrophobic characteristics. A proposed solution-based technique for creating zinc stannate (ZS) and zinc-tin oxide (ZTO) thin films could highlight the advantages of zinc-tin based ternary metal oxides for enhanced photovoltaic parameters.

References

- [1] N. G. Park, “Perovskite solar cells: An emerging photovoltaic technology,” *Mater. Today*, vol. 18, no. 2, pp. 65–72, 2015, doi: 10.1016/j.mattod.2014.07.007.
- [2] W. S. Yang *et al.*, “Iodide management in formamidinium-lead-halide-based perovskite layers for efficient solar cells,” *Science (80-.85)*., vol. 356, no. 6345, pp. 1376–1379, 2017, doi: 10.1126/science.aan2301.
- [3] W. Chen *et al.*, “Efficient and stable large-area perovskite solar cells with inorganic charge extraction layers,” *Science (80-.86)*., vol. 350, no. 6263, pp. 944–948, 2015, doi: 10.1126/science.aad1015.
- [4] J. P. Correa-Baena *et al.*, “Promises and challenges of perovskite solar cells,” *Science (80-.88)*., vol. 358, no. 6364, pp. 739–744, 2017, doi: 10.1126/science.aam6323.
- [5] H. S. Kim *et al.*, “Lead iodide perovskite sensitized all-solid-state submicron thin film mesoscopic solar cell with efficiency exceeding 9%,” *Sci. Rep.*, vol. 2, pp. 1–7, 2012, doi: 10.1038/srep00591.
- [6] Q. Jiang *et al.*, “Enhanced electron extraction using SnO₂ for high-efficiency planar-structure HC(NH₂)₂ PbI₃-based perovskite solar cells,” *Nat. Energy*, vol. 2, no. 1, 2017, doi: 10.1038/nenergy.2016.177.
- [7] T. S. Sherkar *et al.*, “Recombination in Perovskite Solar Cells: Significance of Grain Boundaries, Interface Traps, and Defect Ions,” *ACS Energy Lett.*, vol. 2, no. 5, pp. 1214–1222, 2017, doi: 10.1021/acsenerylett.7b00236.
- [8] T. M. Brenner, D. A. Egger, L. Kronik, G. Hodes, and D. Cahen, “Hybrid organic - Inorganic perovskites: Low-cost semiconductors with intriguing charge-transport properties,” *Nat. Rev. Mater.*, vol. 1, no. 1, 2016, doi: 10.1038/natrevmats.2015.7.
- [9] Y. Fang, C. Bi, D. Wang, and J. Huang, “The Functions of Fullerenes in Hybrid Perovskite Solar Cells,” *ACS Energy Lett.*, vol. 2, no. 4, pp. 782–794, 2017, doi: 10.1021/acsenerylett.6b00657.

- [10] N. J. Jeon *et al.*, “Compositional engineering of perovskite materials for high-performance solar cells,” *Nature*, vol. 517, no. 7535, pp. 476–480, 2015, doi: 10.1038/nature14133.
- [11] N. Moshonas, N. A. Stathopoulos, and G. Pagiatakis, “Optical Modelling of Planar and Fibre Perovskite Solar Cells,” *Electron.*, vol. 11, no. 13, pp. 1–16, 2022, doi: 10.3390/electronics11132041.
- [12] Q. Chen *et al.*, “Controllable self-induced passivation of hybrid lead iodide perovskites toward high performance solar cells,” *Nano Lett.*, vol. 14, no. 7, pp. 4158–4163, 2014, doi: 10.1021/nl501838y.
- [13] Osbel Almora Rodríguez, “Hysteresis and Capacitive Features of Perovskite Solar Cells Osbel Almora Rodríguez,” *Dr. Thesis*, pp. 1–133, 2020.
- [14] E. H. Jung *et al.*, “Efficient, stable and scalable perovskite solar cells using poly(3-hexylthiophene),” *Nature*, vol. 567, no. 7749, pp. 511–515, 2019, doi: 10.1038/s41586-019-1036-3.
- [15] D. Shi *et al.*, “SCIENCE sciencemag.org,” vol. 347, no. 6221, p. 6221, 2015.
- [16] Q. Jiang *et al.*, “Surface passivation of perovskite film for efficient solar cells,” *Nat. Photonics*, vol. 13, no. 7, pp. 460–466, 2019, doi: 10.1038/s41566-019-0398-2.
- [17] J. Seo *et al.*, “Benefits of very thin PCBM and LiF layers for solution-processed p-i-n perovskite solar cells,” *Energy Environ. Sci.*, vol. 7, no. 8, pp. 2642–2646, 2014, doi: 10.1039/c4ee01216j.
- [18] M. Liu, M. B. Johnston, and H. J. Snaith, “Efficient planar heterojunction perovskite solar cells by vapour deposition,” *Nat. 2013 5017467*, vol. 501, no. 7467, pp. 395–398, Sep. 2013, doi: 10.1038/nature12509.
- [19] W. Qiu *et al.*, “Pinhole-free perovskite films for efficient solar modules,” *Energy Environ. Sci.*, vol. 9, no. 2, pp. 484–489, 2016, doi: 10.1039/c5ee03703d.
- [20] C. C. Boyd, R. Checharoen, T. Leijtens, and M. D. McGehee, “Understanding Degradation Mechanisms and Improving Stability of Perovskite Photovoltaics,”

- Chem. Rev.*, vol. 119, no. 5, pp. 3418–3451, 2019, doi: 10.1021/acs.chemrev.8b00336.
- [21] H. Tan *et al.*, “Efficient and stable solution-processed planar perovskite solar cells via contact passivation,” *Science (80-.84)*, vol. 355, no. 6326, pp. 722–726, 2017, doi: 10.1126/science.aai9081.
- [22] K. Wang *et al.*, “Low-temperature and solution-processed amorphous WO₃ as electron-selective layer for perovskite solar cells,” *J. Phys. Chem. Lett.*, vol. 6, no. 5, pp. 755–759, Mar. 2015, doi: 10.1021/ACS.JPCLETT.5B00010/SUPPL_FILE/JZ5B00010_SI_001.PDF.
- [23] T. Leijtens, K. Bush, R. Cheacharoen, R. Beal, A. Bowring, and M. D. McGehee, “Towards enabling stable lead halide perovskite solar cells; interplay between structural, environmental, and thermal stability,” *J. Mater. Chem. A*, vol. 5, no. 23, pp. 11483–11500, Jun. 2017, doi: 10.1039/C7TA00434F.
- [24] G. Niu, X. Guo, and L. Wang, “Review of recent progress in chemical stability of perovskite solar cells,” *J. Mater. Chem. A*, vol. 3, no. 17, pp. 8970–8980, Apr. 2015, doi: 10.1039/C4TA04994B.
- [25] Y. Li *et al.*, “Mesoporous SnO₂ nanoparticle films as electron-transporting material in perovskite solar cells,” *RSC Adv.*, vol. 5, no. 36, pp. 28424–28429, 2015, doi: 10.1039/c5ra01540e.
- [26] H. Cha *et al.*, “An Efficient, ‘Burn in’ Free Organic Solar Cell Employing a Nonfullerene Electron Acceptor,” *Adv. Mater.*, vol. 29, no. 33, p. 1701156, Sep. 2017, doi: 10.1002/ADMA.201701156.
- [27] L. S. Oh *et al.*, “Zn₂SnO₄-based photoelectrodes for organolead halide perovskite solar cells,” *J. Phys. Chem. C*, vol. 118, no. 40, pp. 22991–22994, 2014, doi: 10.1021/jp509183k.
- [28] Z. Galazka *et al.*, “Melt growth and properties of bulk BaSnO₃ single crystals,” *J. Phys. Condens. Matter*, vol. 29, no. 7, 2017, doi: 10.1088/1361-648X/aa50e2.
- [29] A. Kojima, K. Teshima, Y. Shirai, and T. Miyasaka, “Organometal halide

- perovskites as visible-light sensitizers for photovoltaic cells,” *J. Am. Chem. Soc.*, vol. 131, no. 17, pp. 6050–6051, 2009, doi: 10.1021/ja809598r.
- [30] A. Mei, “A hole-conductor-free, fully printable mesoscopic perovskite solar cell with high stability” vol. 295, 2014, doi: 10.1126/science.1254763.
- [31] A. Manuscript, “Materials Chemistry A,” 2016, doi: 10.1039/C6TA07541J.
- [32] W. C. Lai, K. W. Lin, T. F. Guo, P. Chen, and Y. Y. Liao, “Perovskite-based solar cells with inorganic inverted hybrid planar heterojunction structure,” *AIP Adv.*, vol. 8, no. 1, 2018, doi: 10.1063/1.5010951.
- [33] Q. Wang, Q. Dong, T. Li, A. Gruverman, and J. Huang, “Thin Insulating Tunneling Contacts for Efficient and Water-Resistant Perovskite Solar Cells,” *Adv. Mater.*, vol. 28, no. 31, pp. 6734–6739, 2016, doi: 10.1002/adma.201600969.
- [34] J. X. Song, X. X. Yin, Z. F. Li, and Y. W. Li, “Low-temperature-processed metal oxide electron transport layers for efficient planar perovskite solar cells,” *Rare Met.*, vol. 40, no. 10, pp. 2730–2746, 2021, doi: 10.1007/s12598-020-01676-y.
- [35] Q. Q. Ye *et al.*, “UV-Stable and Highly Efficient Perovskite Solar Cells by Employing Wide Band gap NaTaO₃ as an Electron-Transporting Layer,” *ACS Appl. Mater. Interfaces*, vol. 12, no. 19, pp. 21772–21778, 2020, doi: 10.1021/acsami.0c04934.
- [36] X. Li *et al.*, “Rational Design of Solution-Processed Ti-Fe-O Ternary Oxides for Efficient Planar CH₃NH₃PbI₃ Perovskite Solar Cells with Suppressed Hysteresis,” *ACS Appl. Mater. Interfaces*, vol. 9, no. 40, pp. 34833–34843, 2017, doi: 10.1021/acsami.7b08536.
- [37] J. Wei *et al.*, “UV-Inert ZnTiO₃ Electron Selective Layer for Photostable Perovskite Solar Cells,” *Adv. Energy Mater.*, vol. 9, no. 40, pp. 1–7, 2019, doi: 10.1002/aenm.201901620.
- [38] M. Thambidurai, F. Shini, P. C. Harikesh, N. Mathews, and C. Dang, “Highly stable and efficient planar perovskite solar cells using ternary metal oxide electron transport layers,” *J. Power Sources*, vol. 448, no. November 2019, p. 227362, 2020,

doi: 10.1016/j.jpowsour.2019.227362.

- [39] A. E. Shalan, A. N. El-Shazly, M. M. Rashad, and N. K. Allam, “Tin-zinc-oxide nanocomposites (SZO) as promising electron transport layers for efficient and stable perovskite solar cells,” *Nanoscale Adv.*, vol. 1, no. 7, pp. 2654–2662, 2019, doi: 10.1039/c9na00182d.
- [40] N. G. Park, “Organometal perovskite light absorbers toward a 20% efficiency low-cost solid-state mesoscopic solar cell,” *J. Phys. Chem. Lett.*, vol. 4, no. 15, pp. 2423–2429, 2013, doi: 10.1021/jz400892a.
- [41] “Advanced Materials - 2014 - Kim - High-Performance and Environmentally Stable Planar Heterojunction Perovskite Solar Cells.pdf.” .
- [42] Y. You, W. Tian, L. Min, F. Cao, K. Deng, and L. Li, “TiO₂/WO₃ Bilayer as Electron Transport Layer for Efficient Planar Perovskite Solar Cell with Efficiency Exceeding 20%,” *Adv. Mater. Interfaces*, vol. 7, no. 1, pp. 1–9, 2020, doi: 10.1002/admi.201901406.
- [43] H. Choi *et al.*, “Solution-processed ZnO/SnO₂ bilayer ultraviolet phototransistor with high responsivity and fast photoresponse,” *J. Mater. Chem. C*, vol. 6, no. 22, pp. 6014–6022, 2018, doi: 10.1039/c8tc01771a.
- [44] M. Tai *et al.*, “Ultrathin Zn₂SnO₄ (ZTO) passivated ZnO nanocone arrays for efficient and stable perovskite solar cells,” *Chem. Eng. J.*, vol. 361, no. December 2018, pp. 60–66, 2019, doi: 10.1016/j.cej.2018.12.056.
- [45] J. Jiang *et al.*, “Totally room-temperature solution-processing method for fabricating flexible perovskite solar cells using an Nb₂O₅-TiO₂ electron transport layer,” *RSC Adv.*, vol. 8, no. 23, pp. 12823–12831, 2018, doi: 10.1039/c8ra01571f.
- [46] F. Wang *et al.*, “Interface Dipole Induced Field-Effect Passivation for Achieving 21.7% Efficiency and Stable Perovskite Solar Cells,” *Adv. Funct. Mater.*, vol. 31, no. 5, 2021, doi: 10.1002/adfm.202008052.
- [47] R. Meng, X. Feng, Y. Yang, X. Lv, J. Cao, and Y. Tang, “Cerium-Oxide-Modified Anodes for Efficient and UV-Stable ZnO-Based Perovskite Solar Cells,” *ACS Appl.*

- Mater. Interfaces*, vol. 11, no. 14, pp. 13273–13278, 2019, doi: 10.1021/acsami.9b01587.
- [48] H. J. Lee and S. I. Na, “Investigation of PCBM/ZnO and C60/BCP-based electron transport layer for high-performance p-i-n perovskite solar cells,” *J. Alloys Compd.*, vol. 921, p. 166007, 2022, doi: 10.1016/j.jallcom.2022.166007.
- [49] X. Sun, L. Li, S. Shen, and F. Wang, “TiO₂/SnO₂ Bilayer Electron Transport Layer for High Efficiency Perovskite Solar Cells,” *Nanomaterials*, vol. 13, no. 2, 2023, doi: 10.3390/nano13020249.
- [50] N. K. Rana, A. Kumar, N. Chander, and D. S. Ghosh, “Fabrication of a Highly Functional TiO₂/AZO Bilayer Electron Transport Layer for Planar Perovskite Solar Cells,” *ACS Appl. Electron. Mater.*, vol. 5, no. 2, pp. 1050–1056, 2023, doi: 10.1021/acsaem.2c01552.
- [51] Y. W. Noh, I. S. Jin, K. S. Kim, S. H. Park, and J. W. Jung, “Reduced energy loss in SnO₂/ZnO bilayer electron transport layer-based perovskite solar cells for achieving high efficiencies in outdoor/indoor environments,” *J. Mater. Chem. A*, vol. 8, no. 33, pp. 17163–17173, 2020, doi: 10.1039/d0ta04721j.
- [52] Y. Guo *et al.*, “Interface Modification for Planar Perovskite Solar Cell Using Room-Temperature Deposited Nb₂O₅ as Electron Transportation Layer,” *ACS Appl. Energy Mater.*, vol. 1, no. 5, pp. 2000–2006, 2018, doi: 10.1021/acsaem.8b00094.
- [53] B. Yang *et al.*, “Efficient Gradient Potential Top Electron Transport Structures Achieved by Combining an Oxide Family for Inverted Perovskite Solar Cells with High Efficiency and Stability,” *ACS Appl. Mater. Interfaces*, vol. 13, no. 23, pp. 27179–27187, 2021, doi: 10.1021/acsami.1c05284.
- [54] D. Yang *et al.*, “High efficiency planar-type perovskite solar cells with negligible hysteresis using EDTA-complexed SnO₂,” *Nat. Commun.*, vol. 9, no. 1, 2018, doi: 10.1038/s41467-018-05760-x.
- [55] X. Li *et al.*, “A vacuum flash-assisted solution process for high-efficiency large-

- area perovskite solar cells,” *Science* (80-.87)., vol. 353, no. 6294, pp. 58–62, 2016, doi: 10.1126/science.aaf8060.
- [56] M. Leskelä and M. Ritala, “Atomic layer deposition (ALD): From precursors to thin film structures,” *Thin Solid Films*, vol. 409, no. 1, pp. 138–146, 2002, doi: 10.1016/S0040-6090(02)00117-7.
- [57] S. M. George, “Atomic Layer Deposition : An Overview,” pp. 111–131, 2010.
- [58] H. Hu *et al.*, “Atomic Layer Deposition of TiO₂ for a High-Efficiency Hole-Blocking Layer in Hole-Conductor-Free Perovskite Solar Cells Processed in Ambient Air,” *ACS Appl. Mater. Interfaces*, vol. 8, no. 28, pp. 17999–18007, 2016, doi: 10.1021/acsami.6b02701.
- [59] K. T. Cho *et al.*, “Highly efficient perovskite solar cells with a compositionally engineered perovskite/hole transporting material interface,” *Energy Environ. Sci.*, vol. 10, no. 2, pp. 621–627, 2017, doi: 10.1039/c6ee03182j.
- [60] J. Lee *et al.*, “Atomic Layer Deposition of Ultrathin ZnO Films for Hybrid Window Layers for Cu (In x , Ga 1 – x) Se 2 Solar Cells,” pp. 1–10, 2021.
- [61] B. R. Sutherland and E. H. Sargent, “Perovskite photonic sources,” *Nat. Photonics*, vol. 10, no. 5, pp. 295–302, 2016, doi: 10.1038/nphoton.2016.62.
- [62] A. S. Najm *et al.*, “Mechanism of Chemical Bath Deposition of CdS Thin Films: Influence of Sulphur Precursor Concentration on Microstructural and Optoelectronic Characterizations,” *Coatings*, vol. 12, no. 10, 2022, doi: 10.3390/coatings12101400.
- [63] I. R. C. Urbiola, J. A. B. Martínez, J. H. Borja, C. E. P. García, R. R. Bon, and Y. V. Vorobiev, “Combined CBD-CVD technique for preparation of II-VI semiconductor films for solar cells,” *Energy Procedia*, vol. 57, pp. 24–31, 2014, doi: 10.1016/j.egypro.2014.10.004.
- [64] I. Lim *et al.*, “ZnO-CdS Core-shell quantum dots sensitized solar cell: Influence of crystalline and amorphous CdS structures in photovoltaic performance,” *J. Nanosci. Nanotechnol.*, vol. 11, no. 7, pp. 6550–6554, 2011, doi: 10.1166/jnn.2011.4395.

- [65] S. Sengupta, R. Aggarwal, and M. Raula, “A review on chemical bath deposition of metal chalcogenide thin films for heterojunction solar cells,” *J. Mater. Res.*, vol. 38, no. 1, pp. 142–153, 2023, doi: 10.1557/s43578-022-00539-9.
- [66] J. H. Huang *et al.*, “Direct Conversion of $\text{CH}_3\text{NH}_3\text{PbI}_3$ from Electrodeposited PbO for Highly Efficient Planar Perovskite Solar Cells,” *Sci. Rep.*, vol. 5, no. February, pp. 1–8, 2015, doi: 10.1038/srep15889.
- [67] H. Zhu *et al.*, “Preparation of TiO_2 electron transport layer by magnetron sputtering and its effect on the properties of perovskite solar cells,” *Energy Reports*, vol. 8, pp. 3166–3175, 2022, doi: 10.1016/j.egy.2022.02.068.
- [68] H. Niu *et al.*, “Magnetron sputtered ZnO electron transporting layers for high performance perovskite solar cells,” *Dalt. Trans.*, vol. 50, no. 19, pp. 6477–6487, 2021, doi: 10.1039/d1dt00344e.
- [69] M. Kam, Q. Zhang, D. Zhang, and Z. Fan, “Room-Temperature Sputtered SnO_2 as Robust Electron Transport Layer for Air-Stable and Efficient Perovskite Solar Cells on Rigid and Flexible Substrates,” *Sci. Rep.*, vol. 9, no. 1, pp. 1–10, 2019, doi: 10.1038/s41598-019-42962-9.
- [70] Y. Lin and X. Chen, “Electron beam Evaporation Deposition,” *Adv. Nano Depos. methods*, pp. 305–309, 2016.
- [71] M. V. Nikolic *et al.*, “Nanocrystalline $\text{Zn}_2\text{SnO}_4/\text{SnO}_2$: Crystal structure and humidity influence on complex impedance,” *J. Electroceramics*, vol. 45, no. 4, pp. 135–147, 2020, doi: 10.1007/s10832-021-00232-z.
- [72] N. Bai, X. Liu, Z. Li, X. Ke, K. Zhang, and Q. Wu, “High-efficiency TiO_2/ZnO nanocomposites photocatalysts by sol–gel and hydrothermal methods,” *J. Sol-Gel Sci. Technol.*, vol. 99, no. 1, pp. 92–100, 2021, doi: 10.1007/s10971-021-05552-8.
- [73] F. Cao, P. Zhang, and L. Li, “Multidimensional perovskite solar cells,” *Fundam. Res.*, vol. 2, no. 2, pp. 237–253, 2022, doi: 10.1016/j.fmre.2021.07.003.
- [74] A. Loiudice and B. P. G. Niau, “Crystal-Phase Control of Ternary Metal Oxides by Solid-State Synthesis with Nanocrystals,” pp. 2–7, 2022, doi:

10.1021/acsnanoscienceau.1c00049.

- [75] A. Biswal *et al.*, “Role of Additives in Electrochemical Deposition of Ternary Metal Oxide Microspheres for Supercapacitor Applications,” *ACS Omega*, vol. 5, no. 7, pp. 3405–3417, 2020, doi: 10.1021/acsomega.9b03657.
- [76] J. Wang, T. Hasegawa, Y. Asakura, and S. Yin, “Recent Advances in Ternary Metal Oxides Modified by N Atom for Photocatalysis,” *Catalysts*, vol. 12, no. 12, 2022, doi: 10.3390/catal12121568.

Chapter 3

Introduction to Deposition and Characterization Techniques

This chapter has been dedicated to the various deposition and characterization methods that have been employed in this research. It's structured into two fundamental segments: the first pertains to the processes of deposition, and the second delves into the characterization techniques.

3.1 Deposition Methods

3.1.1 Spin Coating

Spin coating is a very common technique for the deposition of thin films. Films can be varied from a thickness of a few nanometers to micrometers, this control of thickness makes it a very effective technique for the deposition of thin films in optoelectronic applications [1].

The spin coating works with the casting of the solution onto the substrate in static or dynamic modes as shown in Figure 3.1. In static mode, the solution is dropped onto the substrate before spinning, whereas in the dynamic mode solution is dropped onto the spinning substrate [2]. Substrates are usually pre-heated for increased adhesion [3]. Spin coating involves the following processes during the thin film deposition:

- The first stage is to drop the solution onto the substrate in dynamic or static modes by using a microliter or a syringe. Solutions are usually filtered before the deposition to avoid the presence of particles which can greatly affect the film uniformity.
- The second stage is also known as the spin-up stage, in which the substrate approaches its max spin speed accelerating at a pre-defined value. This makes the excess fluid on the substrate surface fly off.
- In the third stage, the thinning of the film takes place as the substrate rotates continuously at a constant max speed.

- The fourth stage is when solvent evaporation kicks in. Substrate spins at a constant high speed and the evaporation of solvent makes the film even more thin and uniform.

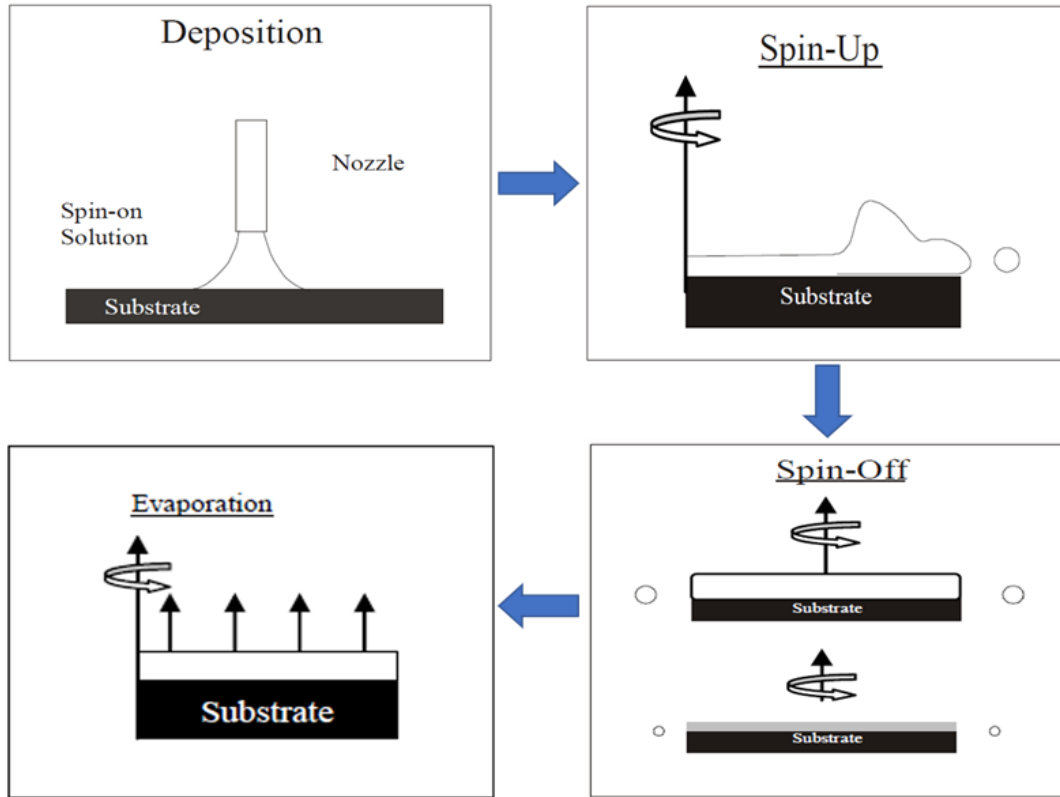


Figure 3.1 Different processes taking place in the spin coating of thin films [4].

Controlling the spin speed and acceleration parameters plays a key role in the uniform deposition of thin films by this deposition technique.

3.1.2 Glove Box

Glove boxes are used in research facilities where the protection of lab researchers against hazardous chemicals or radiations is required. The glove box can also be compared to the fume hoods, where the key difference between them is that fume hoods do not control the internal environment. Whereas glove boxes control the inner environment using oxygen and moisture sensors as shown in Figure 3.2. Also, they are used to provide a nitrogen environment for applications that are very sensitive [5].

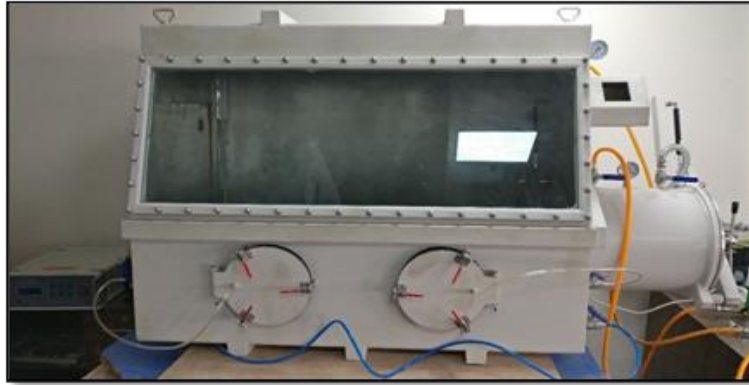


Figure 3.2 Glove Box Setup

Heavy metal sheets, vacuum pumps, and purifiers are used with glove boxes. Oxygen and H₂O levels of up to 0.1 ppm can be achieved. For making inert environment argon or nitrogen gas is used. Specialized rubber gloves are usually used with a glove box for easy maneuverability and protection.

3.1.3 Plasma Cleaning

Plasma cleaning systems are used for the cleaning of FTO substrates in solar cell applications [6]. Plasma cleaners usually consist of a vacuum pump, Inert gas, and oxygen as shown in Figure 3.3. The plasma cleaning process removes all the organic impurities on the surface of a substrate that can affect the film deposition. Moreover, the Surface energy of the substrates is enhanced by plasma treatment that helps in better adhesion of deposited films due to the increased wettability [7].



Figure 3.3 Plasma Cleaner

FTO substrates are placed inside the chamber and the chamber is evacuated by a vacuum pump. Usually, 10-30 minutes are recommended for this process. And cleaned substrates retain their high surface energy for up to 10 minutes. Moreover, it should be noted that plasma treatment only affects the surface properties but not the bulk properties of a substrate [8].

3.2 Characterization Techniques

3.2.1 UV-Vis-NIR Spectroscopy

A spectrophotometer is a device that is used to measure the light absorber by a material at a range of wavelengths. Light is made to strike from one side and the detector is placed on the opposite side to measure the transmitted light. This spectral response of light-absorbing materials especially semi-conductors gives various information like energy band gap, excitation wavelength, etc.

Usually, there are two major types of spectrophotometers. Single beam and double beam. In single beam spectrophotometers, there is a single beam trajectory where there is only one sample placed in the path of light. Whereas in a double beam setup beam is made to pass through two sample holders. Where one can place a reference and a sample side by side for the analysis as shown in Figure 3.4.

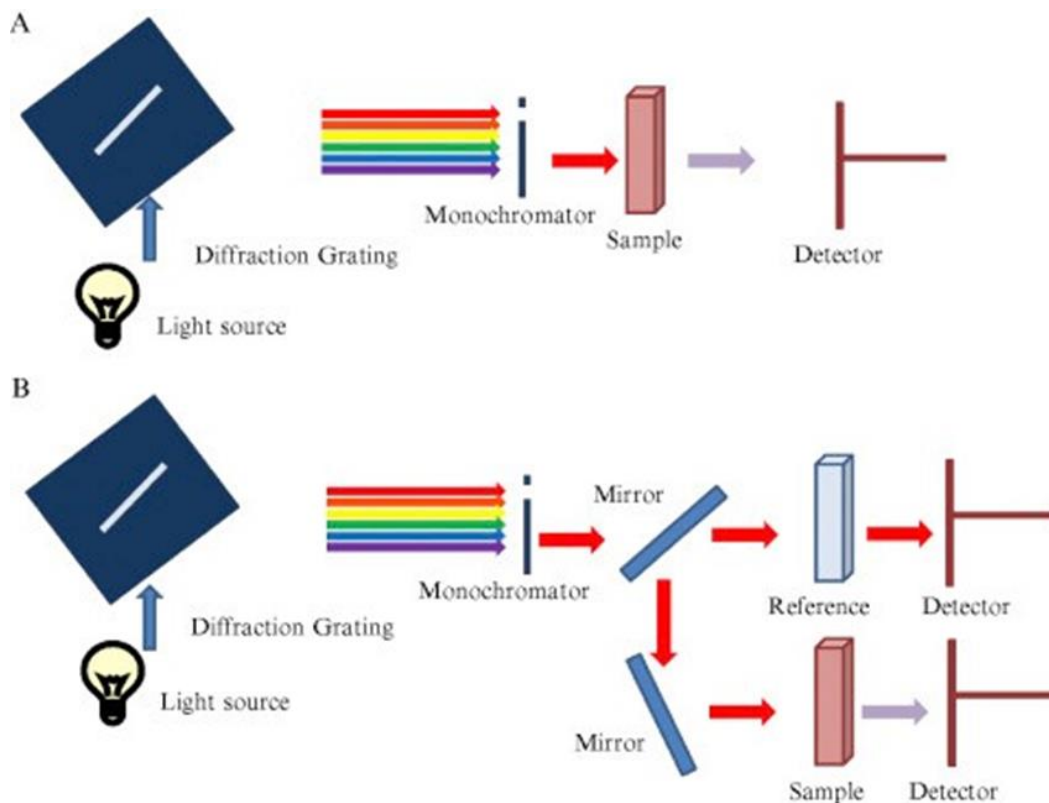


Figure 3.4 Working principle of UV-Vis-NIR spectrophotometer: A) Single beam setup, B) double beam setup [9].

First, a light source produces a beam of light that is made to pass through a grating or monochromator. The light then enters the source and passes through it. A detector placed at the back of the source then detects the remnant light beam. Which is then interpreted and displayed on the computer screen in the form of a spectrum.

3.2.2 Scanning Electron Microscopy (SEM)

Scanning electron microscopy is a widely used surface characterization technique. It uses a beam of highly energetic electrons that hit the sample and generates a 3D image of the sample which gives information on the surface morphology, surface coverage, grain size, etc. [9]. If an EDS accessory is added SEM can also generate information regarding the composition of the deposited thin-film material by sensing the X rays produced due to the inelastic collisions of electrons with the material.

The electron source generates a beam of high-speed electrons at the top of the assembly. Then this beam is accelerated in vacuum conditions to avoid collisions with any foreign atoms. The size of this accelerated beam of electrons is then controlled by the condenser

lenses. Scan coils are used to raster the beam on the sample. Finally, the objective lenses focus the beam on the sample as shown in Figure 3.5.

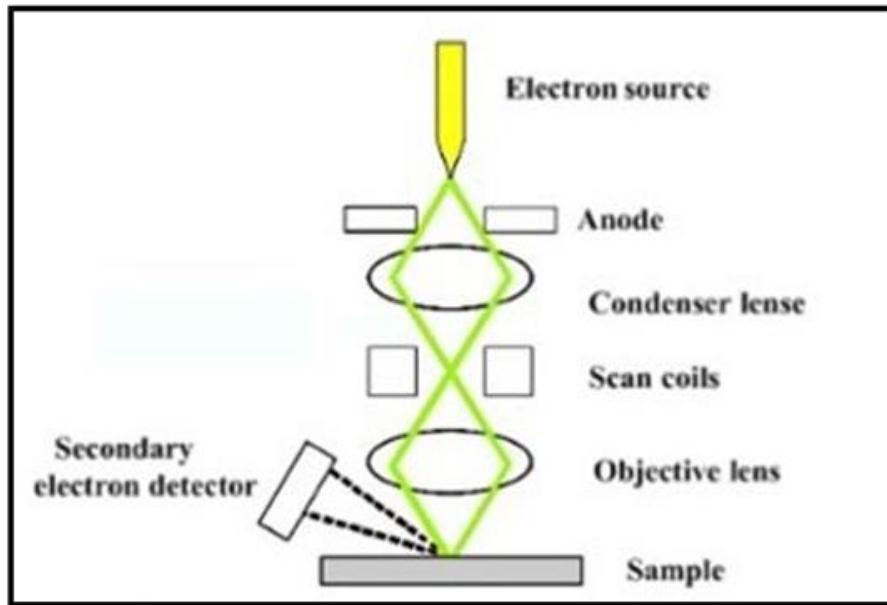


Figure 3.5 Schematic of basic SEM Components [10].

A secondary electron detector is placed at an angle that catches the electrons that are generated by the collision of an electron beam on the sample. These electrons are also known as secondary electrons. Placing the detector at an angle enhances the efficiency of the detector to detect secondary electrons.

3.2.3 X-Ray Diffraction (XRD)

XRD is primarily used to study the crystallographic structure of the materials. It can also be used to determine the crystalline phase, grain size, and unit cell properties of a material. Only crystalline materials can be analyzed by using this technique. Materials are usually finely grounded for analysis. Solid thin films deposited on substrates can also be analyzed [11]. This characterization works based on constructive interference of the X-rays with a crystalline sample as shown in Figure 3.6 [12]. Copper is the most common X-ray source used for the generation of X-rays by bombarding it with high-speed electrons in a cathode ray tube.

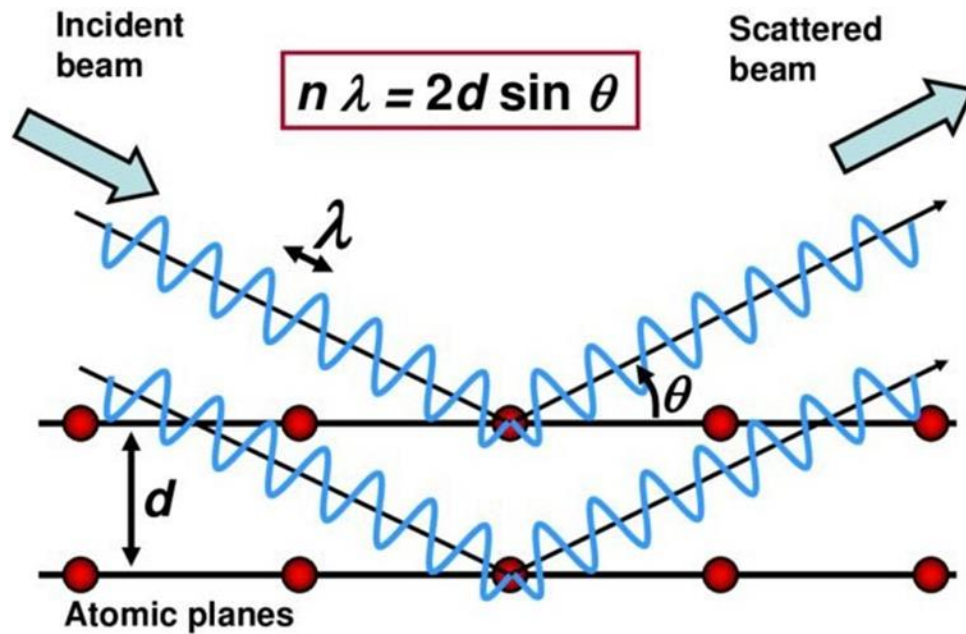


Figure 3.6 Atomic-level illustration of the X-ray interaction with the sample following Bragg's Law [13].

X-rays are then directed towards the sample and a rotating assembly of source and detector is used for detecting the reflected X-rays from the material under analysis. Each X-ray signal is then converted into a count and is plotted against the angle. X-ray detector usually moves at an angle of 2θ . X-rays reflected from the crystal surface elastically. The d-spacing of the crystalline material is determined using Bragg's law as the 2θ angles are already being recorded by the detectors. Knowing all the parameters materials characteristic peaks can be identified from the plotted data.

3.2.4 Hall Effect Measurement System

The Hall effect is used for the measurement of the electrical properties of a thin film. It gives information about charge carrier concentration, sheet resistance, resistivity, and the conductivity of the deposited thin film. It is recommended to prepare hall effect samples on simple glass slides to get an accurate estimate. Charge carriers participating in the flow of current are estimated by this characterization technique.

The hall effect measurement system consists of a magnet, sensing circuit, and a sample placement holder respectively. The sample is placed in the holder with 4 pins that serve as contact points on the thin films. A defined amount of current is passed from the points and

the magnetic field is applied through the magnet. Hall voltage is measured corresponding to the applied current and the magnetic field as shown in Figure 3.7.

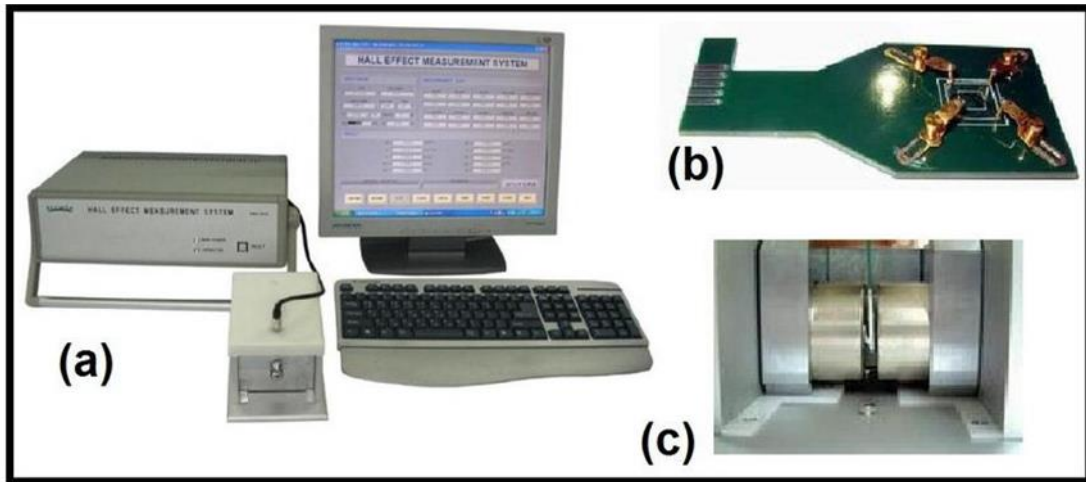


Figure 3.7 Hall Effect Measurement System [14]

The measure of the hall voltage at the point when a balance between the energy of electrons due to an electric and magnetic field is achieved is called the magnetic flux. The relation between the hall voltage and magnetic flux, in turn, gives information about all the other electrical parameters. Special software is used for these calculations that are often incorporated with the system [15]. Very small changes up to mA can be sensed with a hall effect system. Sample dimensions are very important for the accurate measurement of the deposited films. Samples should be prepared in equal square dimensions to collect the correct estimates of charge carriers present in the film.

3.2.5 Contact Angle Measurement System

Contact angle measurement is an analysis technique to analyze the hydrophobic/hydrophilic behavior of a thin film. It can also give estimates about the roughness of a film by analyzing the behavior of solutions on the surface when they meet the solid layer. This instrument measure the angle of contact between solid and liquid phases. Contact angle greater than 90° means the deposited film shows a hydrophobic behavior [16].

The sample is placed on a moveable stage and a water drop of a predefined size in microliters is dropped on the surface of the substrate. A light source illuminates the sample

and the applied droplet. A 60-fps camera placed on the opposite side records a predefined time-stamped video [17]. The brightness of the image can also be manually controlled by a manual dial on the equipment as shown in Figure 3.8. Built-in software tools are then used to trace the boundaries of the droplet and the contact angle is calculated automatically.

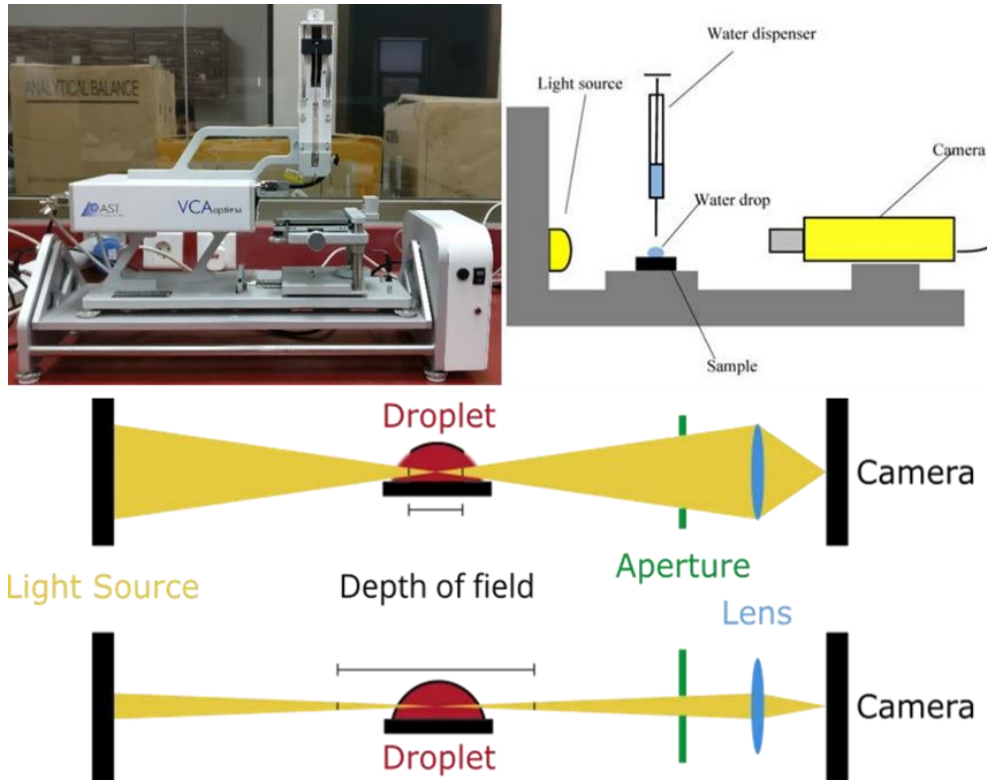


Figure 3.8 Contact angle measurement system working principle schematic [18].

3.2.6 Photoluminescence (PL) Spectroscopy

Photoluminescence spectroscopy also known as PL is a non-contact method of analyzing materials by the interaction of light. It gives information related to bandgaps, recombination mechanisms, molecular structures, impurity and defect detection, and crystallinity. Samples can be used in the form of powder, film, or liquid [19].

It works when the light energy energizes a material to emit a photon. The light is made to fall on the subject material, and it gets absorbed causing photoexcitation in the material. The absorption of a high-energy beam of light causes a jump in the electronic state and a photon (energy) is released when it returns to the lower energy level.

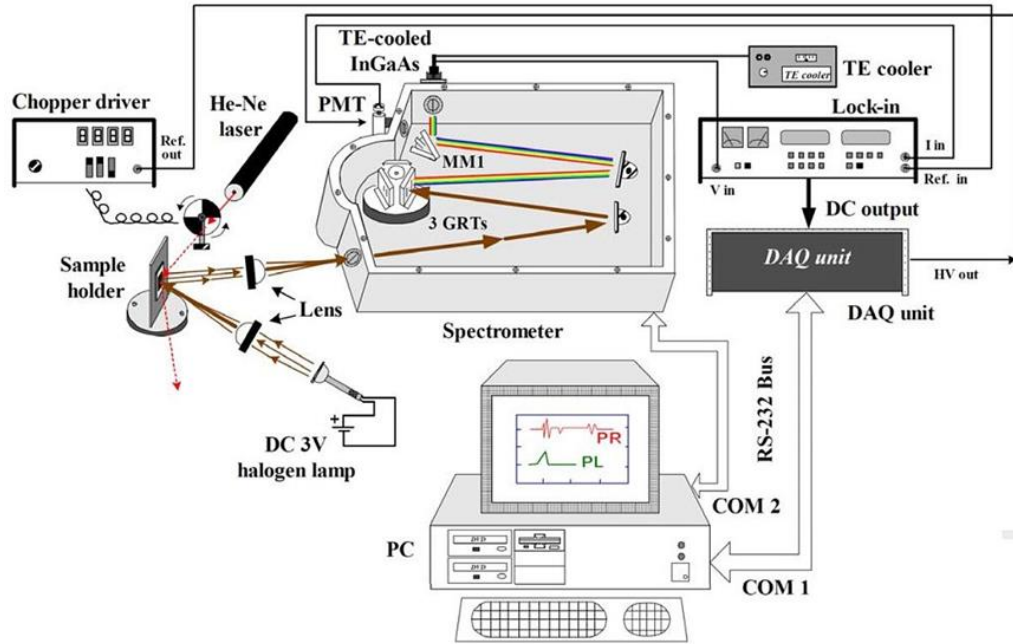


Figure 3.9 Working principle of photoluminescence spectroscopy [20].

This emission of photon or light is called luminescence hence the process of photoluminescence. The recorded emission peaks are further analyzed in built-in software.

Summary

Spin coating is a deposition technique used for the deposition of thin films in solar cells. Controlling the spin speed, acceleration, and time controls the thickness of the deposited films. A very uniform and thin film can be deposited by this technique. The glovebox is used to perform environmentally hazardous and sensitive experiments in the lab. It controls the oxygen and water levels, which can be controlled by using built-in sensors. Spin coaters are usually placed inside the glovebox for solar cell applications that are sensitive to moisture and oxygen-assisted degradation. Plasma cleaners are used to clean the glass substrates used in solar cell applications from organic impurities. UV-Vis-NIR spectroscopy is used to measure the light response of a deposited film on the glass substrate. It gives an idea about the bandgap and absorption wavelength range. Dual-beam setups are used in solar cell applications where glass is placed as a reference. Scanning Electron Microscopy is used to analyze the surface coverage, morphology, and grain size of the material deposited as a thin film in solar cell applications. It uses a highly charged beam of electrons and a detector that senses the backscattered secondary electrons to generate an image.

X-ray Diffraction uses an X-ray source to generate X-rays that are made to contact the sample. Reflected X-rays are detected with the help of a detector and the composition of a sample is analyzed using Bragg's Law. Optical Profilometry is used to measure the thickness of a thin film accurately. It's a non-contact technique that uses a special setup of lenses and a light source to generate topography images of the thin film. The Hall Effect measurement system measures the hall voltage in a thin film when the current is passed through it in the presence of a magnetic field. It gives information about the charge carrier concentration. The contact angle is used to measure the hydrophobicity of a thin film. It uses a drop of deionized water on the surface of the film and a camera records a video to analyze. Photoluminescence is used for non-contact investigation charge transport mechanisms.

References

- [1] N. T. Nguyen, “Micromixers: Fundamentals, Design and Fabrication,” *Micromixers Fundam. Des. Fabr.*, pp. 1–351, Oct. 2011.
- [2] “Cee® Spin Coating Theory - Cost Effective Equipment, LLC.” <https://www.costeffectiveequipment.com/service-support/technical-resources/spin-coating-theory/> (accessed May 08, 2023).
- [3] N. A. A. Mohd Arif, C. C. Jiun, and S. Shaari, “Effect of Annealing Temperature and Spin Coating Speed on Mn-Doped ZnS Nanocrystals Thin Film by Spin Coating,” *J. Nanomater.*, vol. 2017, 2017, doi: 10.1155/2017/2560436.
- [4] D. P. Birnie, “Spin Coating Technology (Common Defects Found When Spin Coating),” 1998, [Online]. Available: <http://www.chematscientific.com/UploadFiles/2016/11/SpinCoating-Introduction.pdf>.
- [5] K. V. Kasiviswanathan, “Hot Cells, Glove Boxes, and Shielded Facilities,” *Encycl. Mater. Sci. Technol.*, pp. 3830–3833, Jan. 2001, doi: 10.1016/B0-08-043152-6/00681-1.
- [6] J. Rao, L. Bao, B. Wang, M. Fan, and L. Feo, “Plasma surface modification and bonding enhancement for bamboo composites,” *Compos. Part B Eng.*, vol. 138, no. November 2017, pp. 157–167, 2018, doi: 10.1016/j.compositesb.2017.11.025.
- [7] A. Y. Kim, J. H. Park, D. Byun, and J. K. Lee, “Effect of oxygen plasma treatment on the electrochemical properties of Prussian blue electrodes for transparent electrochromic devices,” *Thin Solid Films*, vol. 546, pp. 58–62, 2013, doi: 10.1016/j.tsf.2013.05.030.
- [8] Harrick, “Plasma Cleaner: Physics of Plasma,” 2016, [Online]. Available: <https://engineering.jhu.edu/labs/wp-content/uploads/sites/76/2016/04/All-About-Plasma-Cleaning.pdf>.
- [9] C. L. Lin, F. S. Chen, L. J. Twu, and M. J. J. Wang, “Improving SEM inspection performance in semiconductor manufacturing industry,” *Hum. Factors Ergon.*

Manuf., vol. 24, no. 1, pp. 124–129, 2014, doi: 10.1002/hfm.20360.

- [10] “The Applications and Practical Uses of Scanning Electron Microscopes - ATA Scientific.” <https://www.atascientific.com.au/sem-imaging-applications-practical-uses-scanning-electron-microscopes/> (accessed May 08, 2023).
- [11] “X-ray Powder Diffraction (XRD).” https://serc.carleton.edu/research_education/geochemsheets/techniques/XRD.html (accessed May 08, 2023).
- [12] I. F. Cruz, C. Freire, J. P. Araújo, C. Pereira, and A. M. Pereira, *Multifunctional Ferrite Nanoparticles: From Current Trends Toward the Future*. 2018.
- [13] S. Nasir *et al.*, “Potential Valorization of By-product Materials from Oil Palm: A review of Alternative and Sustainable Carbon Sources for Carbon-based Nanomaterials Synthesis,” *BioResources*, vol. 14, no. 1, pp. 2352–2388, 2008.
- [14] “Four Point Probes — Four-Point-Probes offers 4 point probe equipment for measuring the sheet resistance and bulk (volume) resistivity of materials used in the semiconductor industry, universities, and in materials science including thin films, wafers, ingots, and other materials and conductive coatings.” <https://four-point-probes.com/> (accessed May 08, 2023).
- [15] “Definition, Working Principle, Application & Examples of Hall Effect Sensor.” <https://www.elprocus.com/hall-effect-sensor-working-principle-and-applications/> (accessed May 08, 2023).
- [16] M. Abe, “Contact Angle Measurement for Solid Surface,” *Meas. Tech. Pract. Colloid Interface Phenom.*, pp. 129–135, 2019, doi: 10.1007/978-981-13-5931-6_18.
- [17] “Contact Angle Measurement, Theory & Relation to Surface Energy | Ossila.” <https://www.ossila.com/pages/contact-angle-theory-measurement> (accessed May 08, 2023).
- [18] D. Szyszka and W. Szczepanski, “Contact angle of copper-bearing shales using the sessile drop and captive bubble methods in the presence of selected frothers,” *Min.*

Sci., vol. 22, pp. 191–199, 2015, doi: 10.5277/msc152216.

- [19] A. Gao, P. J. Rizo, L. Scaccabarozzi, C. J. Lee, V. Banine, and F. Bijkerk, “Photoluminescence-based detection of particle contamination on extreme ultraviolet reticles,” *Rev. Sci. Instrum.*, vol. 86, no. 6, 2015, doi: 10.1063/1.4922883.
- [20] “Photoluminescence and Photoreflectance - HORIBA.” <https://www.horiba.com/int/scientific/applications/energy/pages/photoluminescence-and-photoreflectance/> (accessed May 08, 2023).

Chapter 4

Experimental Work

This chapter consists of various experimental setups used during this research. It includes solution processing, substrate cleaning, deposition of electron transport layers and absorber layers, etc.

4.1 Materials

Zinc Acetate Dihydrate (CAS No. 5970-45-6), Zinc Chloride (CAS No. 7646-85-7), Tin (II) Chloride Dihydrate (CAS No. 10025-69-1), Tin (II) Chloride (CAS No. 7772-99-8), Methylammonium Iodide (CAS No. 14965-49-2), Lead (II) Iodide (CAS No. 10101-63-0), Cesium Bromide (CAS No. 7787-69-1), 2-Methoxyethanol (CAS No. 109-86-4), N, N Dimethylformamide (CAS No. 68-12-2), Dimethyl sulfoxide (CAS No. 67-68-5) and Fluorine-doped Tin Oxide (FTO) glass substrate were bought from Sigma-Aldrich. All the provided resources were utilized directly, without subjecting them to any additional purification steps.

4.2 Preparation of ETLs

Firstly, the FTO substrates were cleaned through sonication in de-ionized water, 2-propanol, acetone and 2-propanol sequentially for 15 mins each. After sonication, the FTOs were dried using a nitrogen gun and plasma cleaned for 10 mins. ZTO film was synthesized by combining zinc acetate dihydrate ($\text{Zn}(\text{CH}_3\text{COO})_2 \cdot 2\text{H}_2\text{O}$) and tin (II) chloride dihydrate ($\text{SnCl}_2 \cdot 2\text{H}_2\text{O}$) in equal molar proportions, using 2-methoxyethanol (5 ml) as the solvent and adding acetylacetone (100 μl) as a stabilizing agent. After stirring the solution for 3 hours at 60°C, it was spin-coated at 3000 rpm for 30 secs on an FTO substrate followed by annealing at 500° C for 1 hour.

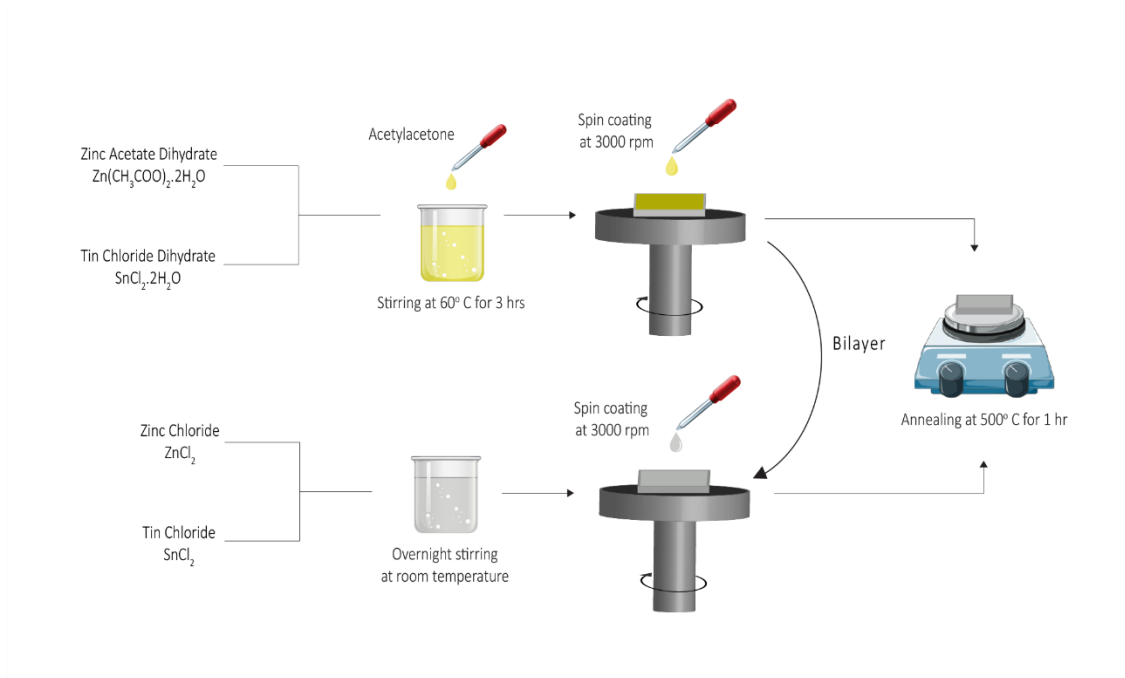


Figure 4.1 Methodology for the preparation of ZTO, ZS and Bilayer electron transport layers.

The colloidal solution for the deposition of ZS thin film was prepared by dissolving 0.2 M of zinc chloride and 0.1 M of tin (II) chloride in ethanol. The precursor solution was stirred overnight at room temperature and deposited onto FTO substrate in the same way as ZTO film. For bilayer, a similar process was repeated for ZTO and ZS film where ZS solution was spin-coated on top of the ZTO film through dynamic mode of operation. Following the deposition of each layer, the substrates were annealed for one hour at a temperature of 500° C. Figure 4.1 provides a clear and concise representation of the systematic methodology involved in the preparation of ternary metal oxide electron transport layers.

4.3 Preparation and Deposition of Absorber Layer

The precursor solution of mixed-cation mixed-halide perovskite absorber layer ($\text{Cs}_{0.1}\text{MA}_{0.9}\text{Pb}(\text{I}_{0.9}\text{Br}_{0.1})_3$) was formulated by adding 461 mg of lead iodide, 143 mg of methylammonium iodide and 21 mg of cesium bromide in 1 ml solvent mixture composed of DMF and DMSO with a volumetric proportion of 4:1. The mixture was stirred at 70° C for 12 hours and filtered through 0.22 μm PTFE filter. The films were deposited onto the ETLs through 2-step spin coating method, initially operated at 500 rpm for 3 secs and then

at 4000 rpm for 30 secs. A schematic representation of the perovskite layer's deposition process is shown in Figure 4.2. During the final 10 seconds of the spinning process, ethyl acetate was added as an anti-solvent. Subsequently, the samples were annealed at 80° C for 40 minutes under the ambient atmosphere.

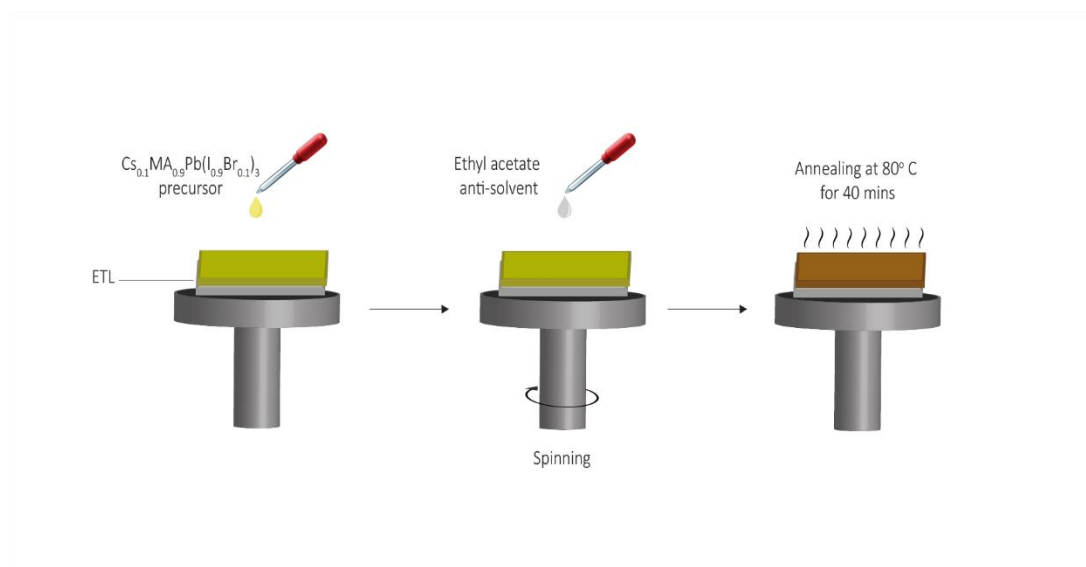


Figure 4.2 Schematic illustration of perovskite layer deposition

4.4 Film Characterizations

Various characterization techniques have been employed to analyze the film structure and morphology, composition, hydrophobic / hydrophilic characteristics and optoelectronic properties.

4.4.1 X-Ray Diffraction (XRD)

The structural properties and crystallite size of ternary metal oxide and perovskite films were examined using the X-ray Diffraction (XRD) method, employing a Bruker D8 Advanced device with a scan cycle of 1.25°/min and a 2-theta range between 10° and 80°. The Cu K α radiation source ($\lambda = 1.542 \text{ \AA}$) was used with a 40 kV excitation voltage and a 30-mA current. Peak analysis and signal processing were performed using Jade 6.5 software from MDI.

4.4.2 Scanning Electron Microscopy (SEM)

The surface morphology of the thin films was investigated with a Scanning Electron Microscope (SEM, JEOL Japan) and images were captured at a 20.0 kV voltage.

4.4.3 UV-Vis-NIR Spectroscopy

To determine the optical properties of ETL and perovskite films, a UV-3600 Plus Ultraviolet–Visible NIR Spectrophotometer was utilized with a 2.5 μm slit width. Transmittance and absorbance measurements were taken in the 250–1100 nm range.

4.4.4 Hall Effect Measurement

To measure the electrical parameters for the deposited electron transport layers, hall effect analysis was conducted. The HMS-3000 hall effect measurement system from ECOPIA was used for this purpose.

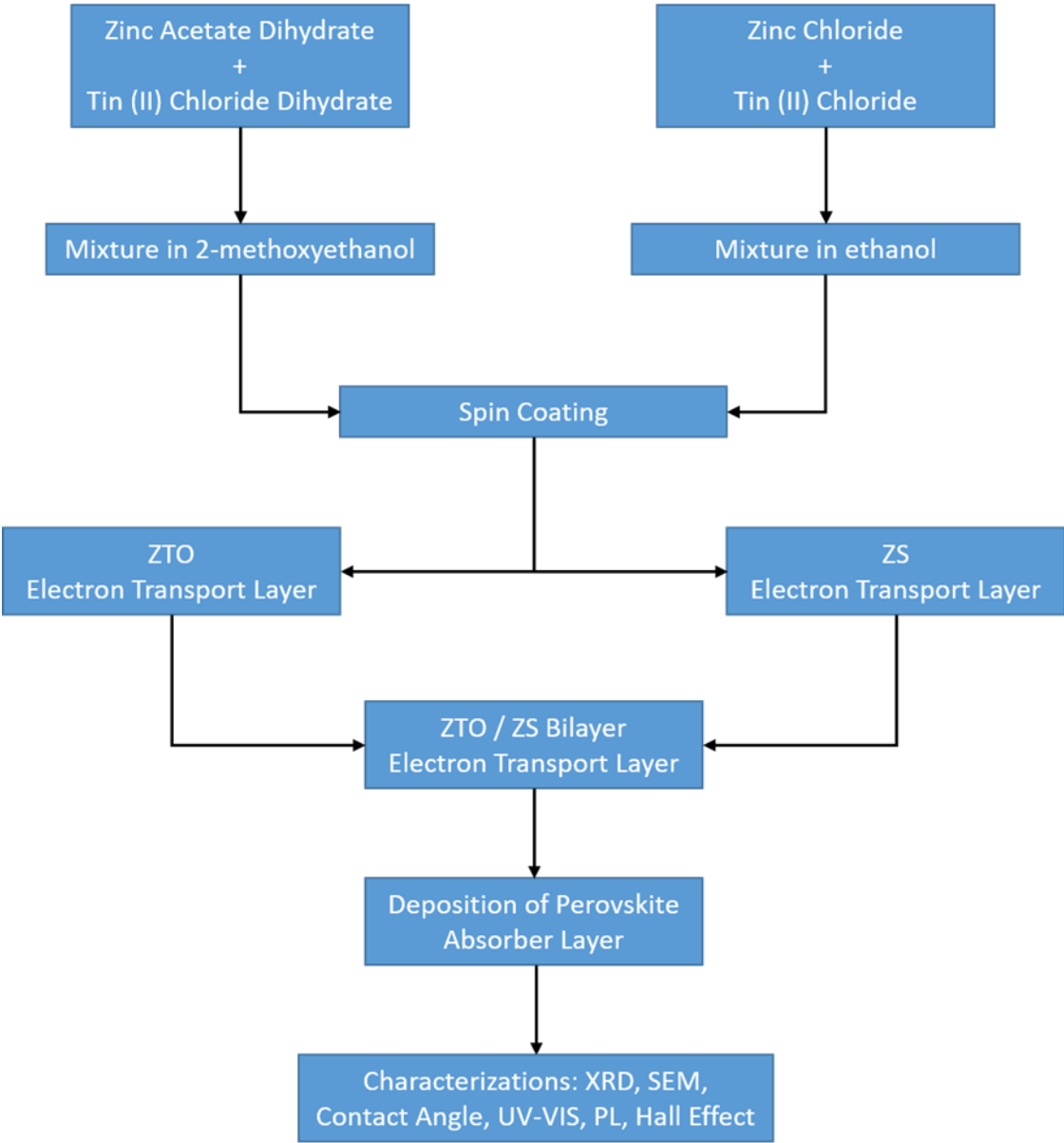
4.4.5 Contact Angle Measurement

The wettability study was performed under ambient conditions with a VCA Optima instrument, utilizing a 30 μL drop of de-ionized water.

4.4.6 Photoluminescence (PL) Analysis

The steady-state photoluminescence (PL) spectra were acquired with an iHR320 spectrophotometer from Horiba Scientific at an excitation wavelength of 450 nm.

Flow Chart



Summary

This chapter outlines the experimental procedures and methods used to prepare and characterize electron transport layers (ETLs) and perovskite absorber layers for solar cells. Various materials were procured from Sigma-Aldrich and used without further purification. The ETLs, consisting of ZTO, ZS, and bilayer films, were prepared through spin-coating and annealing processes. The perovskite absorber layer was formulated using a mixture of lead iodide, methylammonium iodide, and cesium bromide in a DMF/DMSO solvent mixture. The films were deposited onto ETLs using a 2-step spin coating method and annealed.

To characterize the films, multiple techniques were employed. X-ray Diffraction (XRD) was used to analyze the structural properties and crystallite size of the films. Scanning Electron Microscopy (SEM) was employed to study the surface morphology of the thin films. UV-Vis-NIR Spectroscopy was utilized to determine the optical properties of the ETL and perovskite films. Hall Effect measurements were carried out to determine the electrical parameters of the ETLs. Contact Angle measurements were conducted to assess the wettability of the films, and Photoluminescence (PL) Analysis was performed to acquire steady-state PL spectra.

Chapter 5

Results and Discussion

The results and discussion chapter elucidates the findings of the study and interprets their significance in relation to the research objectives. By evaluating the data obtained through various characterization techniques, different surface, structural, electrical, and optical properties of electron transport thin films are presented in detail.

5.1 Structural Analysis

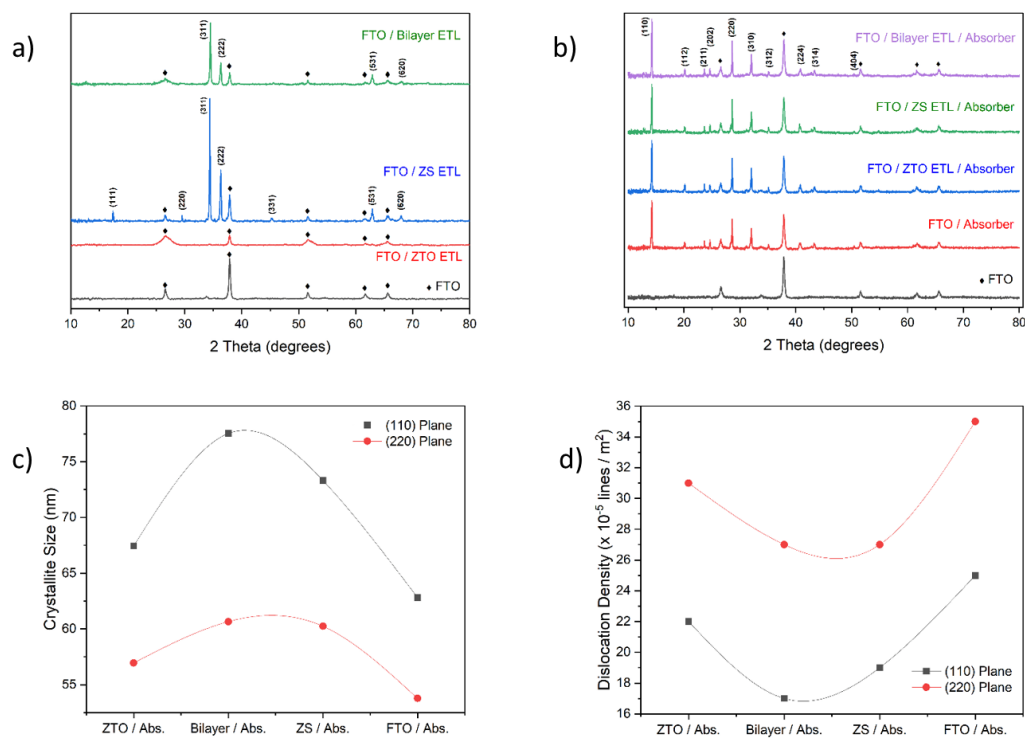


Figure 5.1 XRD Spectra of a) bare FTO, ZTO ETL, ZS ETL and Bilayer ETL. b) Perovskite layer coated on FTO, ZTO ETL, ZS ETL and Bilayer ETL. c) Crystallite Size and d) Dislocation Density of perovskite layer deposited on bare FTO, ZS, ZTO and Bilayer ETLs

XRD analysis was carried out to determine the crystal structure of the deposited films. Figure 5.1a shows the XRD patterns of ZTO, ZS and bilayer films grown on FTO substrate. As previously reported, ZTO, being amorphous in nature, did not show any distinctive crystalline phase as illustrated in Figure 5.2 [1], [2].

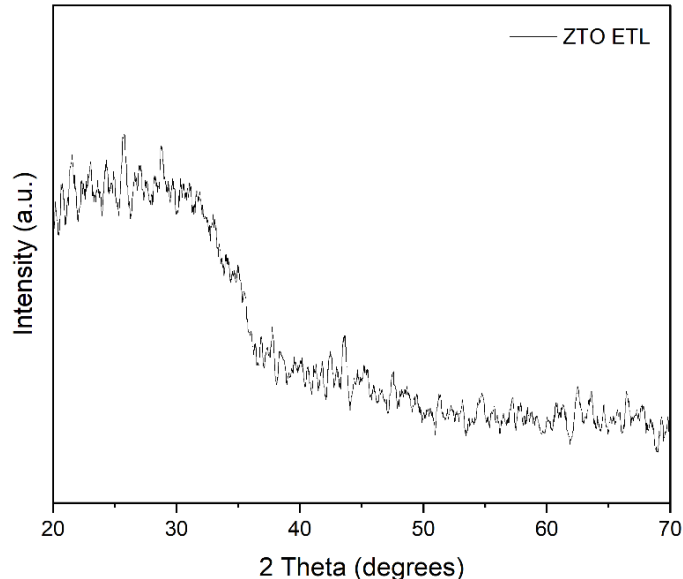


Figure 5.2 XRD Spectrum of ZTO ETL on Glass Substrate

ZTO primarily exhibited a pattern similar to that of FTO, as shown in Figure 5.1a, due to its amorphous thin film [3]. The diffraction peaks observed at 2θ positions of 17.7° , 29.1° , 34.3° , 35.9° , 45.6° , 63.5° and 68.5° corresponds to hkl planes (111), (220), (311), (222), (331), (531) and (620), respectively. These characteristic peaks exhibited a highly crystalline cubic spinel phase structure of zinc stannate (JCPDS No. 24-1470) [4]. In this XRD pattern, there are no distinctive peaks of SnO_2 and ZnO , neither are there any additional diffraction peaks and impurity phases which shows the successful formation of ZS film with no impurities. XRD spectrum of bilayer ETL showed similar structure with slightly less crystallinity.

Figure 5.1b provides the XRD spectra for the highly crystalline $\text{Cs}_{0.1}\text{MA}_{0.9}\text{Pb}(\text{I}_{0.9}\text{Br}_{0.1})_3$ perovskite absorber layer deposited onto the various underlying ETLs. Prominent peaks at 14.2° , 28.6° , and 32.01° can be associated with the (110), (220), and (310) planes of $\text{Cs}_{0.1}\text{MA}_{0.9}\text{Pb}(\text{I}_{0.9}\text{Br}_{0.1})_3$, respectively, meanwhile less intense peaks correspond to (112), (211), (202), (312), (224), (314) and (404) planes, signifying the development of perovskite phase with excellent crystallinity [5]. The absence of the (001) plane for PbI_2

at 12.56° degrees indicates that the PbI₂ had totally dissolved and transformed into the perovskite [6].

Table 2 Crystallographic parameters of perovskite absorber layer deposited on bare FTO, ZS, ZTO and Bilayer ETLs

Sample Name	hkl Planes	FWHM (radians)	Centre (2θ)	Intensity (a.u.)	Crystallite Size (nm)	Dislocation Density (x 10 ⁻⁵ lines.m ⁻²)
CS _{0.1} MA _{0.9} Pb(I _{0.9} Br _{0.1}) ₃	(110)	0.13	14.24	1286.05	62.81	25
	(220)	0.16	28.60	803.85	53.77	35
ZTO /	(110)	0.12	14.24	1380.86	67.45	22
CS _{0.1} MA _{0.9} Pb(I _{0.9} Br _{0.1}) ₃	(220)	0.15	28.60	923.68	56.95	31
ZS /	(110)	0.11	14.24	1276.99	73.32	19
CS _{0.1} MA _{0.9} Pb(I _{0.9} Br _{0.1}) ₃	(220)	0.14	28.60	890.61	60.64	27
Bilayer /	(110)	0.11	14.24	1513.39	77.53	17
CS _{0.1} MA _{0.9} Pb(I _{0.9} Br _{0.1}) ₃	(220)	0.14	28.60	959.12	60.36	27

The mean crystallite size (D) values related to the more intense peaks at (110) and (220) were determined for perovskite layer deposited on FTO as well as ternary metal oxide ETLs employing the widely recognized Debye-Scherrer's equation [7]. The relevant values are presented in Table 2.

$$D = \frac{0.9\lambda}{\beta \cos\theta} \quad \text{Eq. 1}$$

where D represents the mean crystallite size, λ denotes the X-rays wavelength, β signifies the full-width half maxima (FWHM) in radians and θ corresponds to the Bragg's angle. The dislocation density (δ), which can be characterized as the measure of length of dislocation lines within a given volume unit, was also determined for both (110) and (220) peaks using the crystallite size (D) by following equation [8], and the resulting values are presented in Table 2.

$$\delta = \frac{1}{D^2} \quad \text{Eq. 2}$$

Figure 5.1c. indicates a systematic increase in the crystallite size of perovskite films when deposited on ternary metal oxide ETLs, with the greatest increase occurring with bilayer ternary metal oxide ETL. It has been discovered that the dislocation density values for

perovskite films formed on ternary metal oxide ETLs decrease considerably as presented in Figure 5.1d. This larger crystallite size with fewer voids and dislocation densities can improve charge carrier transport resulting in overall better performance of the perovskite solar cells [9].

5.2 Morphological Analysis

The morphological properties of different ternary metal oxide ETLs were studied by taking SEM images as represented in Figure 5.3a-c. A uniform coverage of all the ETLs was observed across the FTO substrate without the presence of any cracks or pinholes. Bilayer ETL, in particular, showed a rather more homogeneous and smoother coverage with comparatively larger grain size which is important for the efficient charge extraction and lower recombinations at the grain boundaries [10], [11].

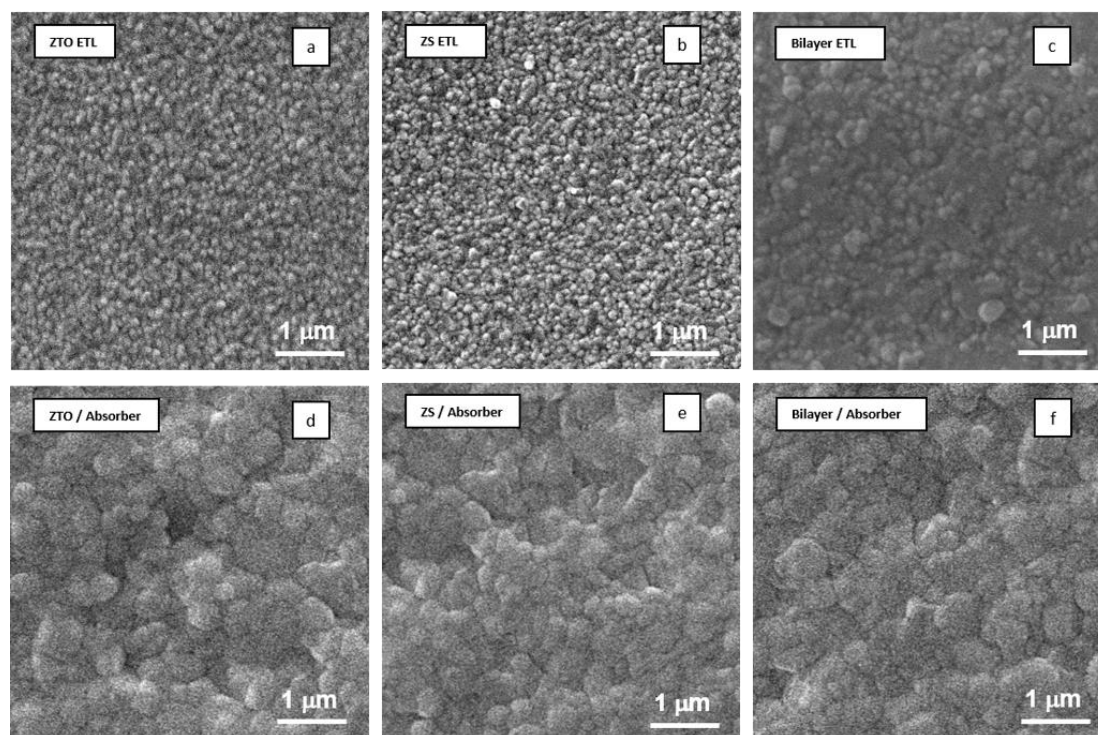


Figure 5.3 Top-view SEM images of (a) ZTO ETL (b) ZS ETL (c) Bilayer ETL coated on FTO substrate. Top-view SEM images of $\text{Cs}_{0.1}\text{MA}_{0.9}\text{Pb}(\text{I}_{0.9}\text{Br}_{0.1})_3$ deposited on (d) ZTO ETL (e) ZS ETL and (f) Bilayer ETL

The top-view SEM images of the $\text{Cs}_{0.1}\text{MA}_{0.9}\text{Pb}(\text{I}_{0.9}\text{Br}_{0.1})_3$ perovskite layer deposited on these ETLs show different surface morphology, as seen in Figure 5.3d-f. Perovskite film grown on ZTO ETL contains pinholes and, therefore, has relatively inferior surface

coverage. Whereas perovskite film deposited on ZS ETL showed better surface coverage with small grains. Notably, when comparing the perovskite films developed on ZTO and ZS ETLs, the perovskite film deposited on bilayer ETL is dense, pinhole-free, and has relatively better surface coverage with larger grain size, as demonstrated in Figure 5.3f. This uniform and highly crystalline perovskite structure on ETL is anticipated to boost the efficiency of PSCs [12].

5.3 Optical and Electrical Properties

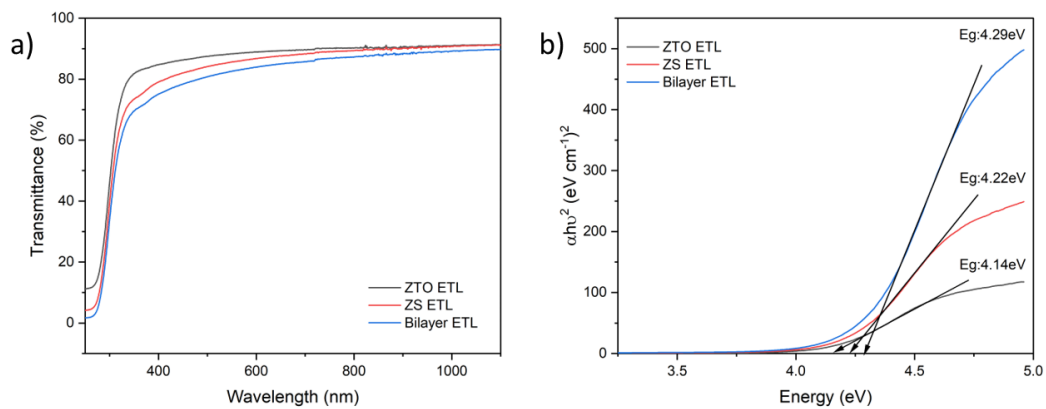


Figure 5.4 (a) Transmittance spectra of ternary metal oxides and bilayer ETLs. (b) Tauc plots of ternary metal oxides and bilayer ETLs

To study the optical properties, the transmittance spectra of ternary metal oxides and bilayer ETLs have been obtained on the glass substrate, and represented in Figure 5.4a. ZTO ETL, in particular, exhibited higher transmittance in the Visible range. This permits ZTO ETL to transfer a greater amount of incoming light to the perovskite layer, thereby improving the light capture efficiency within PSCs. ZS ETL demonstrated relatively lower transmittance as it was produced from a colloidal solution. Whereas the optical transmittance of bilayer ETL is decreased due to the multiple reflections and transmissions occurring at the interfaces between the two layers.

The tauc plots in Figure 5.4b depicts the optical bandgaps of 4.14 eV and 4.22 eV for ZTO and ZS ETLs respectively. The bandgap of bilayer ETL was increased to 4.29 eV. This increased bandgap is associated with more chemical and thermal stability [13].

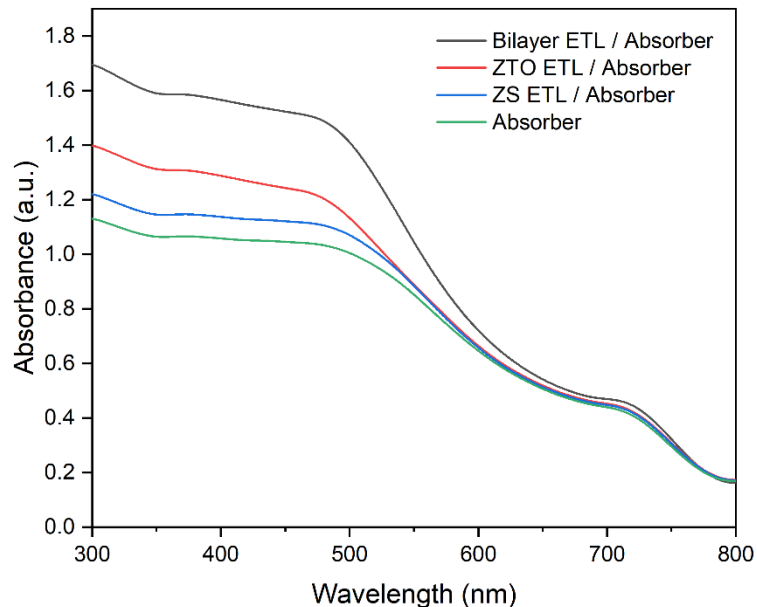


Figure 5.5 Absorbance spectra of perovskite film coated on glass, ZTO, ZS and Bilayer ETLs

The absorbance spectra of perovskite films over glass or different ETL substrates are almost similar, as shown in Figure 5.5. Perovskite film deposited on bilayer ETL exhibited the highest absorption values due to large grain size and high surface coverage ratio, as supported by the SEM results in Figure 5.3f. These high absorption values with bilayer ETL are crucial for superior device performance and elevated current densities [14]. In addition, the absorber layer deposited on glass and other ETLs has the same absorption pattern with a prominent absorption peak at $\sim 745\text{nm}$, which is attributed to the $\text{Cs}_{0.1}\text{MA}_{0.9}\text{Pb}(\text{I}_{0.9}\text{Br}_{0.1})_3$ perovskite layer [15].

Urbach energy, also known as the Urbach tail or Urbach edge, is often used to measure the quality of a semiconductor film and is correlated with electronic disorders present in the film. Generally, lower Urbach energy values indicate a lower degree of electronic disorders, showing higher quality films with fewer defects and inhomogeneities [16], [17]. Figure 5.6 presents the Urbach energy values of $\text{Cs}_{0.1}\text{MA}_{0.9}\text{Pb}(\text{I}_{0.9}\text{Br}_{0.1})_3$ perovskite film deposited on glass and other ETLs.

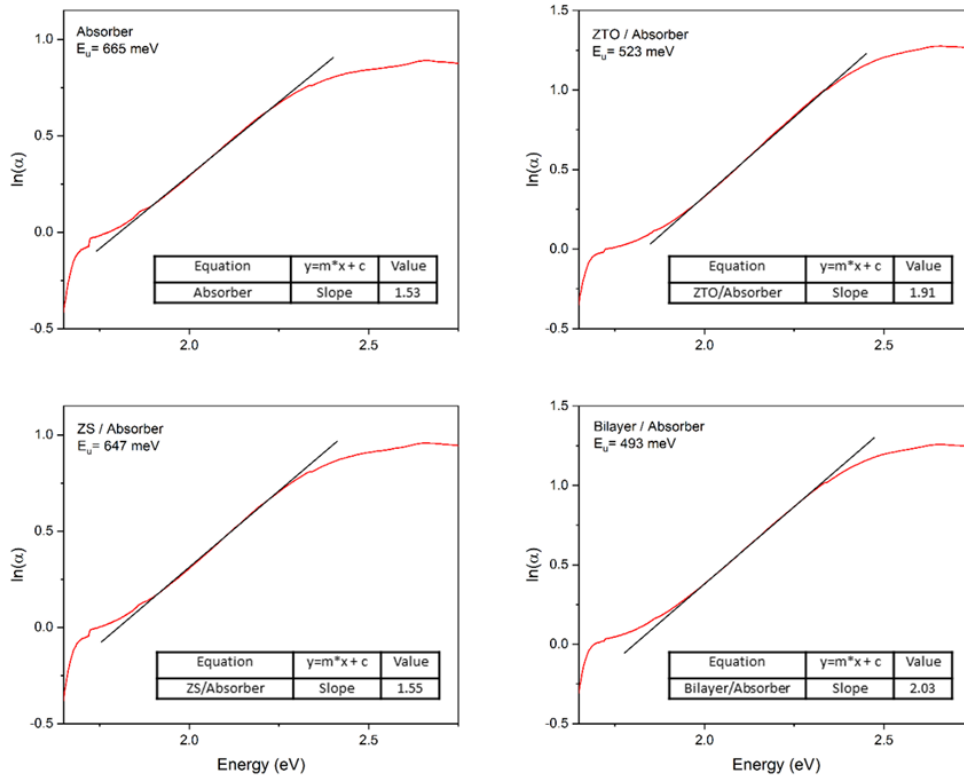


Figure 5.6 Urbach Energies (E_u) of perovskite film coated on glass and different ETLs

These Urbach energy values were obtained from inverse slope of the graph plotted between $\ln(\alpha)$ and photon energy ($h\nu$) where α is the absorption coefficient that was determined by the following equation [18]

$$\alpha = 2.303 \left(\frac{A}{t} \right) \quad \text{Eq. 3}$$

here A denotes the absorbance and t represents thickness of the film. An overall reduction in the Urbach energy values of perovskite film is observed when deposited on ZTO, ZS and bilayer ETLs. However, the lowest Urbach energy was recorded with bilayer ETL, indicating the highest quality of absorber layer with least electronic abnormalities. This reduction of Urbach energy is associated with the least dislocation density values, as presented in Table 2, and the growth of large perovskite crystals as evident from the morphological analysis of perovskite absorber layer deposited on bilayer ETL. Larger crystallite size with fewer grain boundaries can reduce the density of defect states and improve the carrier transport properties, leading to lower Urbach energy values [19].

Table 3 Hall Effect parameters of different ternary metal oxide based ETLs

Sample Name	Bulk Concentration ($\times 10^{21} \cdot \text{cm}^{-3}$)	Mobility ($\text{cm}^2 \cdot \text{V}^{-1} \cdot \text{s}^{-1}$)	Sheet Resistance ($\Omega \cdot \text{square}^{-1}$)	Conductivity ($\text{W}^{-1} \cdot \text{cm}^{-1}$)
ZS	-6.841	15.84	11.52	1.736
ZTO	-7.046	15.39	11.51	1.738
Bilayer	-4.987	21.84	11.46	1.745

The investigation of the electrical properties of ETLs were conducted at room temperature through Hall effect measurements, with the findings presented in Table 3. The negative values of bulk concentration indicate n-type nature of the charge carriers. The electron mobilities of ZS and ZTO ETLs exhibit near-identical values of $15.84 \text{ cm}^2 \text{V}^{-1} \text{s}^{-1}$ and $15.39 \text{ cm}^2 \text{V}^{-1} \text{s}^{-1}$, respectively, which is consistent with prior studies [20]. Meanwhile, the mobility of the bilayer ETL is increased to $21.84 \text{ cm}^2 \text{V}^{-1} \text{s}^{-1}$, with a slight enhancement in conductivity. The improvement in charge carrier mobility of bilayer film is attributed to its comparatively smoother coverage as discussed in SEM analysis. This relatively smooth surface reduces scattering and other obstacles that can impede the motion of the charge carriers which leads to more effective electron transport and extraction [21].

5.4 Photoluminescence Analysis

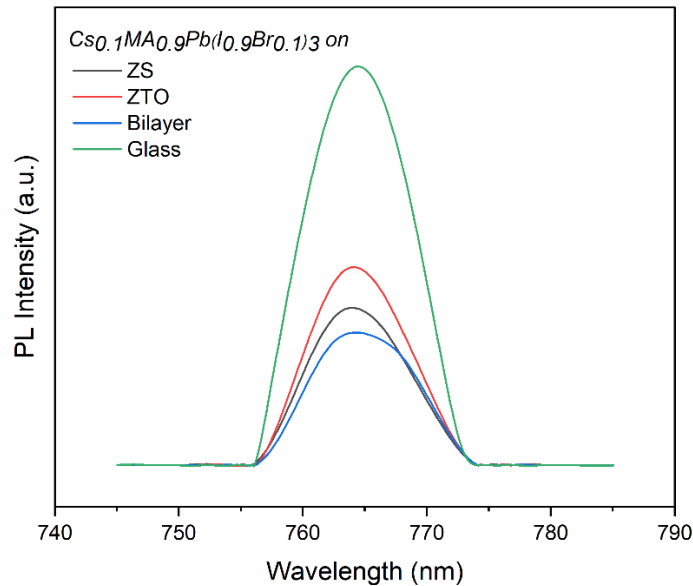


Figure 5.7 Photoluminescence spectrum of the perovskite film on Glass, ZTO, ZS and Bilayer ETLs

The PL studies were conducted to measure the electron extraction efficiency of each layer from perovskite absorber layer. Figure 5.7 illustrates the steady-state PL quenching spectra of perovskite films deposited on different substrates. The gradual decrease in the PL intensity signifies the charge extraction efficiency of each layer which is maximum for bilayer ETL. This implies that bilayer ETLs are most efficient to extract electrons from the perovskite layer as compared to others.

5.5 Wettability Study

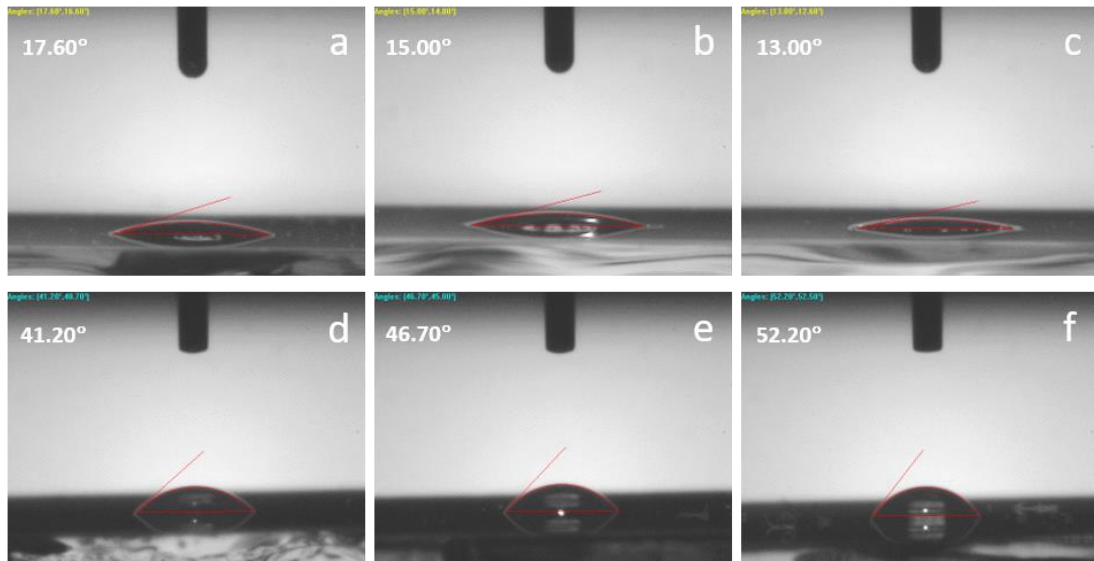


Figure 5.8 Water contact angle of (a) ZS ETL (b) ZTO ETL (c) Bilayer ETL and water contact angle of $CS_{0.1}MA_{0.9}Pb(I_{0.9}Br_{0.1})_3$ perovskite film deposited on (d) ZS ETL (e) ZTO ETL and (f) Bilayer ETL

Contact angle analysis was conducted in order to study the hydrophilic nature and wettability of different layers. Figure 5.8 shows the contact angle values of ETLs and subsequent perovskite films. The contact angle measurements for bare glass substrate indicated in Figure 5.9a, has a fairly hydrophilic character with the contact angle of 30.90° .

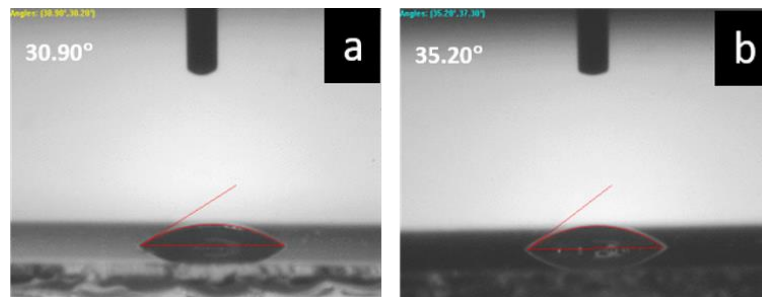


Figure 5.9 Water contact angle of (a) bare glass substrate and (b) pristine perovskite film deposited on glass substrate

The contact angle reduces significantly with the deposition of ETLs indicating increased hydrophilicity. Notably, the bilayer ETL exhibits the minimum contact angle of 13.00° which is beneficial for subsequent deposition of $\text{Cs}_{0.1}\text{MA}_{0.9}\text{Pb}(\text{I}_{0.9}\text{Br}_{0.1})_3$ perovskite film as it leads to an increase in surface energy and expedites the crystallization process for the growth of perovskite structure [22]. The lower water contact angle is also due to smooth and uniformly deposited bilayer ETL visible through SEM.

Moreover, morphological analysis suggests that larger crystallite size in perovskite layer can result in fewer grain boundaries, which reduces the potential sites for moisture-induced degradation and improves the layer's resistance against moisture [23]. From Figure 5.8d-f, it can be seen that the contact angle for perovskite film grown on different ETL samples, particularly bilayer ETL, is remarkably greater than the pristine perovskite film (Figure 5.9b) which indicates a higher resistance to erosion by moisture and, consequently, a higher level of device stability [24].

Summary

This chapter investigates the structural, morphological, optical, and electrical properties of electron transport thin films. The study focuses on zinc stannate, zinc tin oxide, and bilayer films grown on FTO substrate, as well as the properties of $\text{Cs}_{0.1}\text{MA}_{0.9}\text{Pb}(\text{I}_{0.9}\text{Br}_{0.1})_3$ perovskite absorber layers. Key findings include improved crystallite size and reduced dislocation densities in perovskite films deposited on ternary metal oxide ETLs, particularly bilayer ETL. SEM analysis reveals uniform ETL coverage, with bilayer ETL exhibiting smoother surfaces, which contribute to enhanced charge carrier mobility. Optical analysis indicates bilayer ETLs possess higher bandgaps, while photoluminescence measurements reveal superior charge extraction and transport capabilities. Wettability studies show bilayer ETLs have lower contact angles, indicating improved hydrophilic nature and better resistance to moisture-induced degradation.

References

- [1] T. Z. Oo *et al.*, “Zinc Tin Oxide (ZTO) electron transporting buffer layer in inverted organic solar cell,” *Org. Electron.*, vol. 13, no. 5, pp. 870–874, 2012, doi: 10.1016/j.orgel.2012.01.011.
- [2] M. Thambidurai, F. Shini, P. C. Harikesh, N. Mathews, and C. Dang, “Highly stable and efficient planar perovskite solar cells using ternary metal oxide electron transport layers,” *J. Power Sources*, vol. 448, no. November 2019, p. 227362, 2020, doi: 10.1016/j.jpowsour.2019.227362.
- [3] L. Kadri *et al.*, “Optical and Structural Analysis of TiO₂ – SiO₂ Nanocomposite Thin Films Fabricated via Pulsed Laser Deposition Technique,” 2023.
- [4] F. Sadegh *et al.*, “Highly efficient, stable and hysteresis–less planar perovskite solar cell based on chemical bath treated Zn₂SnO₄ electron transport layer,” *Nano Energy*, vol. 75, no. April, p. 105038, 2020, doi: 10.1016/j.nanoen.2020.105038.
- [5] H. Choi *et al.*, “Cesium-doped methylammonium lead iodide perovskite light absorber for hybrid solar cells,” *Nano Energy*, vol. 7, pp. 80–85, 2014, doi: 10.1016/j.nanoen.2014.04.017.
- [6] G. Tumen-Ulzii *et al.*, “Detrimental Effect of Unreacted PbI₂ on the Long-Term Stability of Perovskite Solar Cells,” *Adv. Mater.*, vol. 32, no. 16, pp. 1–7, 2020, doi: 10.1002/adma.201905035.
- [7] N. H. Toudjjen, B. Bendahmane, M. L. Zeggar, F. Mansour, and M. S. Aida, “SnO₂ thin film synthesis for organic vapors sensing at ambient temperature,” *Sens. Bio-Sensing Res.*, vol. 11, pp. 52–57, 2016, doi: 10.1016/j.sbsr.2016.11.001.
- [8] G. Turgut and E. Sönmez, “Synthesis and characterization of Mo doped SnO₂ thin films with spray pyrolysis,” *Superlattices Microstruct.*, vol. 69, pp. 175–186, 2014, doi: 10.1016/j.spmi.2014.02.009.
- [9] B. Chen *et al.*, “Grain Engineering for Perovskite/Silicon Monolithic Tandem Solar Cells with Efficiency of 25.4%,” *Joule*, vol. 3, no. 1, pp. 177–190, 2019, doi: 10.1016/j.joule.2018.10.003.

- [10] C. Lu, W. Zhang, Z. Jiang, Y. Zhang, and C. Ni, “Graphene quantum dots doping SnO₂ for improving carrier transport of perovskite solar cells,” *Ceram. Int.*, vol. 47, no. 21, pp. 29712–29721, 2021, doi: 10.1016/j.ceramint.2021.07.143.
- [11] S. Pang *et al.*, “Boosting performance of perovskite solar cells with Graphene quantum dots decorated SnO₂ electron transport layers,” *Appl. Surf. Sci.*, vol. 507, no. October 2019, 2020, doi: 10.1016/j.apsusc.2019.145099.
- [12] T. Cao, K. Chen, Q. Chen, Y. Zhou, N. Chen, and Y. Li, “Fullerene Derivative-Modified SnO₂ Electron Transport Layer for Highly Efficient Perovskite Solar Cells with Efficiency over 21%,” *ACS Appl. Mater. Interfaces*, vol. 11, no. 37, pp. 33825–33834, 2019, doi: 10.1021/acsami.9b09238.
- [13] L. C. Tien and C. H. Ho, *Synthesis, optical characterization, and environmental applications of β -Ga₂O₃ nanowires*. Elsevier Inc., 2018.
- [14] Y. J. Kim *et al.*, “Enhanced Light Harvesting in Photovoltaic Devices Using an Edge-Located One-Dimensional Grating Polydimethylsiloxane Membrane,” *ACS Appl. Mater. Interfaces*, vol. 11, no. 39, pp. 36020–36026, 2019, doi: 10.1021/acsami.9b09377.
- [15] X. Liu *et al.*, “Stable Pure Iodide MA_{0.95}Cs_{0.05}PbI₃ Perovskite toward Efficient 1.6 eV Bandgap Photovoltaics,” *J. Phys. Chem. Lett.*, pp. 5088–5093, 2022, doi: 10.1021/acs.jpcllett.2c01356.
- [16] M. Ledinsky *et al.*, “Temperature Dependence of the Urbach Energy in Lead Iodide Perovskites,” *J. Phys. Chem. Lett.*, vol. 10, no. 6, pp. 1368–1373, 2019, doi: 10.1021/acs.jpcllett.9b00138.
- [17] S. Singh *et al.*, “Effect of Thermal and Structural Disorder on the Electronic Structure of Hybrid Perovskite Semiconductor CH₃NH₃PbI₃,” *J. Phys. Chem. Lett.*, vol. 7, no. 15, pp. 3014–3021, 2016, doi: 10.1021/acs.jpcllett.6b01207.
- [18] R. R. T. and B. K. Singh, “Absorbance and Transmittance measurement of CsI thin film,” *Proc. DAE Symp. Nucl. Phys.*, vol. 58, pp. 838–839, 2013.
- [19] F. Wang, S. Bai, W. Tress, A. Hagfeldt, and F. Gao, “Defects engineering for high-

- performance perovskite solar cells,” *npj Flex. Electron.*, vol. 2, no. 1, 2018, doi: 10.1038/s41528-018-0035-z.
- [20] S. S. Shin *et al.*, “High-performance flexible perovskite solar cells exploiting Zn₂SnO₄ prepared in solution below 100 °C,” *Nat. Commun.*, vol. 6, no. May, pp. 1–8, 2015, doi: 10.1038/ncomms8410.
- [21] M. Geiger *et al.*, “Effect of the Degree of the Gate-Dielectric Surface Roughness on the Performance of Bottom-Gate Organic Thin-Film Transistors,” *Adv. Mater. Interfaces*, vol. 7, no. 10, 2020, doi: 10.1002/admi.201902145.
- [22] H. V. Quy and C. W. Bark, “Ni-Doped SnO₂ as an Electron Transport Layer by a Low-Temperature Process in Planar Perovskite Solar Cells,” *ACS Omega*, vol. 7, no. 26, pp. 22256–22262, 2022, doi: 10.1021/acsomega.2c00965.
- [23] H. Mao *et al.*, “Surface grain boundary passivation via mixed antisolvent and PC 61 BM assistant for stable perovskite solar cells,” *J. Mater. Sci. Mater. Electron.*, vol. 30, no. 4, pp. 3511–3520, 2019, doi: 10.1007/s10854-018-00628-8.
- [24] R. Chen *et al.*, “Carbon-based HTL-free modular perovskite solar cells with improved contact at perovskite/carbon interfaces,” *J. Mater. Chem. C*, vol. 8, no. 27, pp. 9262–9270, 2020, doi: 10.1039/d0tc02226h.

Chapter 6

Conclusions and Recommendations

This chapter lays out various outcomes that are derived from this whole research. Also, some future outlooks are discussed to conduct further research on the topic.

6.1 Conclusions

In conclusion, this research has thoroughly investigated the structural and morphological characteristics, optical aspects and electrical properties of solution-processed ternary metal oxide films as potential ETLs for PSCs. XRD and SEM analyses demonstrated that perovskite film crystallite size and morphology were enhanced when deposited on ternary metal oxide ETLs, particularly in bilayer compositions. These ETLs exhibited uniform coverage across the substrate, signifying efficient charge extraction. Optical measurements revealed high transmittance in the visible region and a bandgap range of 4.14 eV - 4.29 eV. Furthermore, photoluminescence analysis indicated superior charge extraction and transportation in the bilayer ETL with perovskite absorber layer, while contact angle analysis revealed increased resistance to moisture erosion and improved device stability. Hall effect measurements confirmed n-type conductivity of the films, with enhanced charge transport and extraction observed in the bilayer ETL. This study highlights the potential of zinc-tin based ternary metal oxides as effective electron transport layers in high-efficiency, stable planar perovskite solar cells.

6.2 Future Recommendations

For the future work, the following suggestions are recommended to fabricate a complete working device in ambient conditions based on ternary metal oxide-based perovskite solar cells (PSCs):

- Investigate the impact of different growth conditions (temperature, pressure, and deposition methods) on the properties of ternary metal oxide ETLs and bilayer ETLs to optimize their performance.

- Develop strategies to minimize the impact of grain boundaries and defect states on the performance of perovskite solar cells, possibly through the use of passivation techniques or novel material engineering approaches.
- Explore other novel ternary metal oxide compositions or multilayered ETLs to further enhance the efficiency and overall performance of perovskite solar cells.
- Examine the potential of integrating bilayer ternary metal oxide ETLs into tandem or multi-junction solar cells to achieve higher overall device efficiencies.

Summary

This chapter presents the conclusions and future recommendations derived from the research on solution-processed ternary metal oxide films as potential electron transport layers (ETLs) for perovskite solar cells (PSCs). The study demonstrates enhanced crystallite size and morphology of perovskite films when deposited on ternary metal oxide ETLs, particularly bilayer compositions. These ETLs exhibited uniform coverage, efficient charge extraction, high transmittance, and increased resistance to moisture erosion. Future recommendations include investigating the impact of growth conditions on ETL properties, minimizing the impact of grain boundaries and defect states, exploring novel ternary metal oxide compositions, and examining the integration of bilayer ETLs into tandem or multi-junction solar cells for improved efficiency.

Appendix-A: Journal Article

Solution-Processed Zn₂SnO₄ / ZTO Electron Transport Layers for Planar Perovskite Solar Cells

Saad Nadeem^a, *Nadia Shahzad^a, Sana Mehmood^a, Muhammad Salik Qureshi^a, Abdul Sattar^b, Rabia Liaquat^a, Sehar Shakir^a, Muhammad Imran Shahzad^c

^a*U.S.-Pakistan Centre for Advanced Studies in Energy (USPCAS-E), National University of Sciences & Technology (NUST), H-12 Sector (44000) Islamabad, Pakistan*

^b*Energy Matériaux Telecommunications Research Center, Institut National de la Recherche Scientifique (INRS-EMT), Quebec, Canada*

^c*Nanosciences and Technology Department (NS&TD), National Centre for Physics (NCP), 44000 Islamabad, Pakistan*

*Corresponding Author's Email: nadia@uspcase.nust.edu.pk

ABSTRACT

Perovskite solar cells (PSCs) have acquired popularity owing to their high efficiency, ease of fabrication, and affordability. In this context, the development of electron transport layers (ETLs) for highly efficient planar photovoltaic devices has received considerable attention. This study investigates the potential of zinc-tin based ternary metal oxide ETLs for application in planar PSCs. Solution-processed methods were used to fabricate crystalline zinc stannate (Zn₂SnO₄), amorphous zinc-tin oxide (ZTO), and Zn₂SnO₄ / ZTO based bilayer films, and their structural, morphological, and optoelectronic properties were studied. XRD and scanning electron microscopy images showed enhanced crystallite size and better surface morphology of perovskite films deposited on bilayer ETL. These ETLs exhibited uniform coverage and high transmittance of up to 90% in the visible spectrum with a band gap range from 4.14 eV for ZTO ETL to 4.29 eV for bilayer ETL. Whereas Photoluminescence studies and Hall effect measurements revealed superior charge extraction, an improved charge carrier mobility (21.84 cm²V⁻¹s⁻¹) and enhanced n-type conductivity in the bilayer ETL. Moreover, contact angle analysis of perovskite layer deposited on bilayer ETL showed increased resistance to moisture erosion (52.20°) which is particularly significant given the detrimental effects moisture can have on the performance of PSCs.

Keywords: ternary metal oxides, electron transport layer, bilayer, ambient fabrication, perovskite solar cells

Appendix-B: Journal Article

Effect of lanthanum doped SnO₂ on the performance of mixed-cation mixed-halide perovskite for planar PSCs

Sana Mehmood^a, *Nadia Shahzad^a, Saad Nadeem^a, Muhammad Salik Qureshi^a, Abdul Sattar^b, Naseem Iqbal^a, Rabia Liaquat^a, Muhammad Imran Shahzad^c

^a*U.S.-Pakistan Centre for Advanced Studies in Energy (USPCAS-E), National University of Sciences & Technology (NUST), H-12 Sector (44000) Islamabad, Pakistan*

^b*Energy Matériaux Telecommunications Research Center, Institut National de la Recherche Scientifique (INRS-EMT), Quebec, Canada*

^c*Nanosciences and Technology Department (NS&TD), National Centre for Physics (NCP), 44000 Islamabad, Pakistan*

*Corresponding Author's Email: nadia@uspcase.nust.edu.pk

ABSTRACT

Perovskite solar cells (PSCs) have attracted significant attention due to their higher efficiencies and lower fabrication costs. But for the better performance of PSCs, a high-quality electron transport layer (ETL) is crucial. Various ETLs have been employed and among them Tin (IV) oxide (SnO₂) has emerged as a promising candidate for electron selective layer in PSCs due to its superior optical and electrical characteristics. However, there is still improvement needed in terms of poor surface morphology and conductivities of SnO₂. When SnO₂ is used in conjunction with absorber layer in ambient conditions, stability, and charge carrier recombinations at SnO₂/perovskite interface remains a serious challenge as well. This study presents the doping of lanthanum (La III), a rare earth element, into SnO₂ ETLs to improve the quality and performance of the perovskite layer deposited on top of ETL in ambient condition. With the optimized 4% La (III) doping, SnO₂ ETLs become more crystalline with lower parasitic light absorption and surface morphology improves significantly. The improvement in morphology due to doping facilitates larger crystal growth of perovskite in ambient environment. Moreover, Photoluminescence reveals that with optimized level of doping, interfacial charge recombinations are significantly mitigated ensuring smooth injection of electrons into ETL because of superior perovskite film quality. The mixed-cation mixed-halide perovskite film deposited on 4% La-doped ETL show better resistance towards moisture ingress and will substantially contribute to develop long-life of planar PSCs.

Keywords: electron transport layer, mixed-cation, mixed-halide, perovskite, ambient fabrication, elemental doping